GROWTH AND CHARACTERIZATION OF CDTE/ZNTE THIN FILMS AND HETEROSTRUCTURES

GROWTH AND CHARACTERIZATION OF CDTE/ZNTE THIN FILMS AND HETEROSTRUCTURES

BY CARLEY MIKI, B.Sc

A Thesis Submitted to the School of Graduate Studies in Partial Fulfilment of the Requirements for the Degree Master of Science

McMaster University Master of Science (2014) Hamilton, Ontario (Physics)

TITLE: Growth and Characterization of CdTe/ZnTe Thin Films and Heterostructures

AUTHOR: Carley Miki, B.Sc. (University of Guelph)

SUPERVISOR: Professor John S. Preston

NUMBER OF PAGES: ix, 100

Abstract

CdTe and ZnTe are common semiconductors, currently used in a wide variety of applications. Heterostructures, composed of two or more layered materials, create further potential for the use of these semiconductors in the development of new technologies. In this thesis, the epitaxial growth of CdTe/ZnTe thin films and heterostructures are studied with the intention of better understanding the mechanisms by which they grow and how their overall structure and properties may be modified. Single-layer, bilayer, and multilayer structures were grown by pulsed laser deposition on sapphire substrates. The resulting crystal structure, interface, and optical properties were characterized using X-ray diffraction, UV-Vis spectroscopy, atomic force microscopy, and electron microscopy and spectroscopy techniques. It was found that the growth conditions have a direct impact on the crystal quality of these materials, that can be understood in terms of the growth dynamics and film-substrate interactions. Domain formation was also found to vary between CdTe and ZnTe depositions, revealing important information about their growth. This work presents methods of consistently producing high quality CdTe and ZnTe thin films and bilayers, and insight into how this may be applied to the growth of multilayer films.

Acknowledgements

Contents

List of Figures

List of Tables

Chapter 1

Introduction

Studies of thin film semiconductors are of interest from both a technological and scientific perspective. These materials are currently used in many device applications, and the increased surface area-to-volume ratio and introduction of size effects can have a drastic impact on the properties of the same material compared to bulk form, revealing interesting physical phenomenon. Because of this, much work in recent decades has been done to both better understand these systems and develop novel materials.

CdTe and ZnTe are common II-VI semiconductors, widely used in current technologies because of their structural and optical properties. For instance, the high optical absorption coefficient and nearly ideal band gap for efficient photovoltaic conversion makes CdTe an excellent candidate for thin film solar cells [4] [5], and its heavy constituent elements and high electron mobility when doped has drawn attention as gamma-ray and x-ray detectors used in the medical industry and nuclear research [6][7][8]. Similarly, the direct band gap of ZnTe, which lies in the visible wavelength region, makes it a common material choice for light-emitting diodes, photodetectors, and semiconductor lasers [9]. The properties that make CdTe and ZnTe so desirable are dependent on internal atomic structure, and so an understanding of what is responsible for the formation of this structure is important. Perhaps of more interest is

understanding how this knowledge may be applied to modify the structure and thereby tune the resulting properties of the material.

Heterostructured thin films, composed of two or more layered materials that interact at an interface, allow additional opportunities for tuning and open up exciting new areas of physics and device engineering. CdTe/ZnTe heterostructures are of particular interest because of their visible wavelength band gaps, which makes them suitable for optoelectronic devices [10]. CdTe/ZnTe heterostructures have also received attention as potential tandem solar cell components, which are able to absorb a wider range of the solar spectrum than traditional CdTe solar cells [11][12]. Quantum well structures can also be fabricated by layering a thin CdTe film between two thicker ZnTe films. These structures are currently being used for various applications including diode lasers, photodetectors, and optical modulators [13]. However, the interface between the layered materials frequently causes irregularities in the structural and electronic properties of the heterostructure as a whole due to factors such as strain, dislocations, defects, and interdiffusion [14]. It is therefore necessary to study the role of the interface in heterostructures and their impact on material properties.

In this work, CdTe and ZnTe thin films grown by pulsed laser deposition are studied. Bilayer films are fabricated to investigate the CdTe/ZnTe interface in preparation for the fabrication of multilayer films, containing many CdTe/ZnTe interfaces. X-ray diffraction (XRD), ultraviolet-visible spectroscopy (UV-Vis), scanning electron microscopy (SEM), transmission electron microscopy (TEM), Auger electron spectroscopy (AES) and atomic force microscopy (AFM) are used for characterization.

1.1   Thin Films

Thin films encompass a wide variety of materials and have found applications in many different fields. These all share the feature that one dimension is much smaller than the other two, and because of this, can exhibit properties much different than those possessed by their bulk counterparts. In bulk materials, the majority of the atoms are contained within the volume of the material. Each of these atoms experiences roughly the same environment as every other atom in the solid, and is acted on by the same net forces. The exception are those atoms which lie on the surface. These atoms see a much different environment, since there is nothing to interact with above the plane of the surface. Thin films differ from bulk materials in that a much greater fraction of the atoms are on the surface instead of in the volume. The increased surface area-to-volume ratio gives rise to many unique properties resulting from changes to surface state energies, crystal structure, etc. [15]. In very thin films, electrons are confined to two-dimensions, which further effects the electronic properties of the material by changing the density of states and available energy levels. In addition, well established models for describing solids fail to explain the behaviour of thin films, as the assumption that contributions from surface atoms are negligible when compared to contributions from the bulk is no longer valid [16].

The study of these properties and their dependence on the dimensions of a material has driven the development of novel technologies and fabrication processes. As a desire for smaller and faster electronics has grown, so has the study of thin films to accomplish this. Integrated circuits depend on thin film technology, with the development of components like transistors benefiting from this technology. In addition, use as coatings for applications in optics, environment, and energy, have come to rely on thin films [15][17]. Improvements in thin film solar cells would not be possible without a thorough understanding of the physics and fabrication of these materials. The development of ultra-high vacuum technology and deposition systems are also consequences of thin film

research [16]. Because of these reasons and many others, thin films remain an important topic in research, with new discoveries and models continuing to inspire advanced technologies and applications.

1.2   Epitaxy

The growth of materials possessing uniform crystal structure is crucial to the study and development of thin films. Defects and impurities, which cause irregularities in the crystal structure, can have a detrimental impact on the properties of the material. Because of this, a highly regular structure is desired.

Epitaxy is the growth of a crystalline film on top of a crystalline substrate, with the orientation and atomic spacings of the film being dictated by the underlying lattice. This allows for the growth of high quality materials with long-range atomic ordering. However, the substrate and film lattices need to be compatible in structure and orientation in order for this process to be successful. The easiest way to guarantee this is to grow a film on top of a substrate of the same material. This is referred to as homoepitaxy and constitutes the vast majority of epitaxy work accomplished to date. A match between different materials can still result in epitaxial growth, and is referred to as heteroepitaxy. In this case, the film and substrate likely do not share the same lattice constant, but instead slightly differ. The lattice mismatch at the interface can be calculated as the percent-difference between the lattice constants of the film, a_1 and the substrate a_2:

$$\frac{a_1 - a_2}{a_2} \tag{1.1}$$

The mismatch causes a strain in the film as the lattice is distorted to accommodate the substrate. If the mismatch is small enough (typically $< 4\%$), the system has little strain and behaves like a homoepitaxial system, but if the strain is great enough, the film may either propagate the strain from the interface through the entire lattice, resulting in a strained film, or else form

defects at the interface to alleviate the strain, resulting in a strain-relaxed film [17]. These different scenarios are depicted in Fig. 1.1 for comparison.
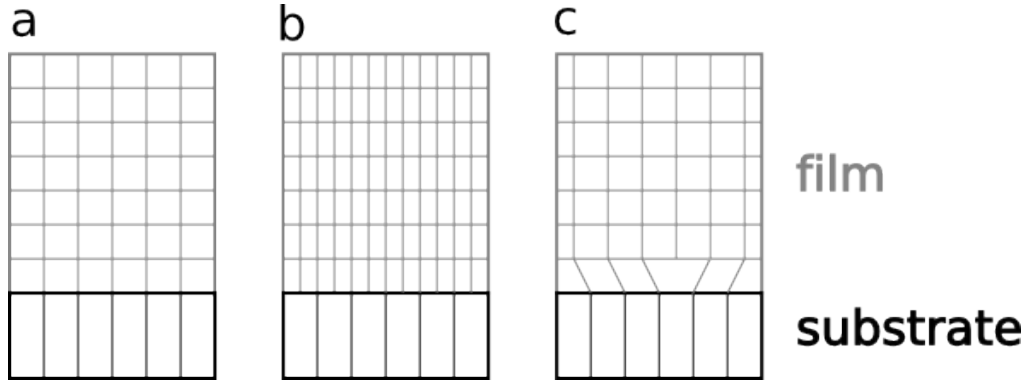
Figure 1.1: Schematic representation of a film-substrate interface that is a) lattice matched and fully relaxed, b) lattice mismatched and strained, and c) lattice mismatched and strain-relaxed.

The formation of defects in semiconductors is challenging to overcome. Since many device properties, such as carrier mobility and absorption/emission processes, are altered by the presence of defects, fabricating high quality materials with a low defect density is of interest. Misfit dislocations are defects that form during the growth of an epitaxial film that causes the regular ordering of the atoms to be interrupted. This commonly originates from stress but can also be caused by contamination or other existing defects. In a lattice mismatched system, the two main competing energies at the interface, the elastic energy and the dislocation energy, dictate whether a misfit dislocation will form. The elastic energy originates from the lattice deformation the film undergoes in an attempt to accommodate the underlying lattice of the substrate. This energy increases as the thickness of the film increases, and dominates the response of very thin films. As the thickness increases, the elastic energy becomes greater, and at some critical thickness d_c, it will become energetically favourable for a misfit dislocation to form. This reduces the elastic energy and the overall energy of the system, which is the sum of the elastic and dislocation energies.

The critical thickness depends on the degree of mismatch between the film and substrate as well as the Young's modulus and shear modulus of the film material. These defects usually form in the plane parallel to the film-substrate interface and typically have the highest density near the interface. As the film continues to grow it will relax as the lattice is no longer strained due to the misfit dislocations previously formed [17] [18].

Another growth defect common in epitaxial films comes from the nucleation of multiple domains with different crystallographic orientations. The domains eventually meet as the film thickness increases, resulting in a grain boundary. In this thesis, the domains form such that the grains have the same crystal structure but are misaligned relative to each other. This defect is referred to as a twin, with the twin boundary acting as a mirror plane between the grains. For example, if the regular stacking sequence in a film is A-B-C-A-B-C, a twinned film might have the sequence A-B-C-A-B-A-C-B-A, with the boundary occurring at the second B plane. The stacking sequence on either side of the plane will be mirror images of each other. The origin of this type of defect is not well understood, but it has been suggested that its formation may be reversed if the growth temperature is high enough to promote sufficient diffusion. Stacking faults, which form when a plane in the regular staking sequence is either inserted or missing, also commonly occur in epitaxial growth [17]. An example of this type of defect would result in a stacking sequence such as A-B-C-A-B-A-B-C.

1.3   Growth Dynamics

Epitaxial films have been fabricated for many years as a way of producing consistently high quality materials. Several different techniques are used to accomplish this, but they all rely on the same physical principles when describing the processes that occur at the film-substrate interface.

When an atom interacts with the substrate surface, there are several processes it may undergo. Fig. 1.2 depicts these processes, which will be described in detail below.
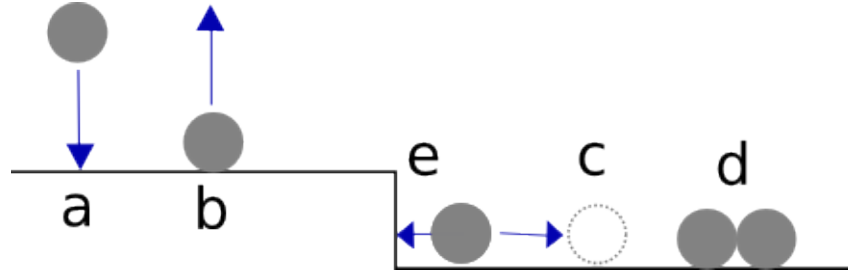
Figure 1.2: The processes an adatom may undergo during epitaxial growth: a) absorption, b) desorption, c) surface diffusion, d) nucleation, and e) step-binding.

The first of these processes is adsorption. This involves an atom in the vapour phase bonding to the surface of the substrate. The rate at which this occurs depends on the adsorption coefficient of the particular atom and the rate the atoms arrive at the substrate. The adsorption coefficient represents the percentage of arriving atoms that form adatoms, and the arrival rate is a combination of the number of atoms in the vapour and the velocity of each [19]. If the average velocity or the total number of atoms is increased, the rate of adsorption will be greater.

It is also possible that an adatom, originally bonded to the substrate, will desorb and be reincorporated into the vapour. The average lifetime, τ_A, an adatom experiences on the surface of the substrate is described as

$$\tau_A = \nu_A^{-1} exp(\frac{E_A}{k_B T}) \tag{1.2}$$

where ν_A is a prefactor on the order of thermal oscillations in the lattice, E_A is the desorption activation energy, k_B is Boltzmann's constant $(1.3806 \times 10^{-23} \frac{m^2 kg}{s^2 K})$ and T is the temperature at the substrate [19][15]. If the temperature at the substrate surface is increased, the average lifetime will decrease, meaning more

7

adatoms desorb. This is an important factor to consider, since the mean lifetime can become very short at high enough temperatures, inhibiting the growth of a film.

An adatom also has the option of diffusing to nearby sites on the substrate. The probability that an adatom diffuses is given by

$$t_D = \nu_D^{-1} exp(\frac{E_D}{k_B T}) \tag{1.3}$$

where ν_D is the prefactor for this process, and E_D is the activation energy for diffusion. This implies that at higher temperatures there is a greater probability that an adatom diffuses. The distance that it diffuses, λ, can be described in terms of the diffusion coefficient D, and the mean lifetime spent on the substrate [19]

$$\lambda = \sqrt{D\tau_A} \tag{1.4}$$

Surface diffusion is important in the growth of epitaxial films since this provides a mechanism for the adatoms to adapt to their changing environment and attempt to minimize surface energies.

Adatoms may also incorporate into steps in the surface that grow as more atoms are deposited. The growth rate of a straight step, v_s is given by

$$v_s = 2\sigma\lambda\chi I_e\Phi \tag{1.5}$$

where σ is the surface area, λ is the diffusion length of the adatom, χ is the absorption coefficient, Φ is the supersaturation of the vapour over the substrate, and I_e is the equilibrium deposition rate [19].

As more atoms adsorb onto the substrate, they begin to interact with each other and ultimately grow into an epitaxial film. The growth mechanism through which this occurs depends on many factors, including the balance of kinetic processes described above, but generally falls into one of three major categories: island growth (Volmer-Weber), layer-by-layer growth (Frank van der Merwe), and the intermediate layer-plus-island growth (Stranski-Krastanov) [20].
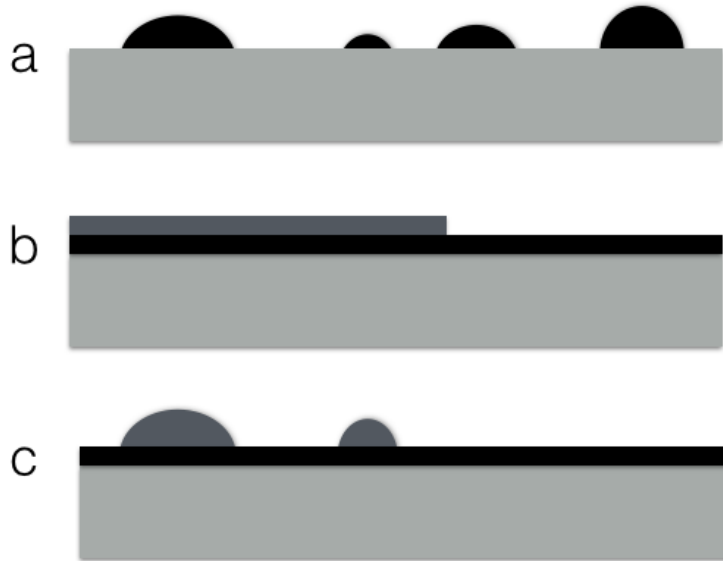
Figure 1.3: Growth modes associated with epitaxial films: a) island b) layer-by-layer c) layer-plus-island

Island growth usually occurs when the deposited atoms are more strongly attracted to themselves than the substrate. Small clusters (eg. dimers or trimers) nucleate at various points on the substrate surface, and subsequent atoms tend to group around these points. The result is a series of islands that grow and eventually coalesce as more material is deposited. In contrast, layer-by-layer growth arises when the deposited atoms are more strongly attracted to the substrate, so the atoms tend to cover the surface before growing upwards. Layer-plus-island is a combination of the other two modes, and results in the formation of a complete layer, with island growth on top. This is most often the case in strained systems, where the interfacial energy changes with film thickness [20]. A schematic comparison of these modes is shown in Fig. 1.3. The rate at which the film grows also depends on a number of other variables such as the substrate temperature, the type of interacting atoms, etc., and is strongly dependent on the growth mode used [19].

1.4   Properties of CdTe and ZnTe

1.4.1   Crystal Structure

II-VI compounds such as CdTe and ZnTe are composed of two types of atoms, with each atom being tetragonally bonded to 4 other atoms of the opposite type. The constituent atoms are bonded covalently, with some ionic character because of the two types of atoms differing in charge (eg. Cd^{+2} and Te^{-2}) [21]. This forms the basis of two crystal structures: zinc blende and wurtzite. The symmetries of these structures are very different, with zinc blende having a cubic crystal structure, and wurtzite having a hexagonal crystal structure. These differences allow the structures to be distinguished using characterization tools such as X-ray diffraction. This technique will be discussed in later sections, and the difference in the zinc blende and wurtzite powder patterns for CdTe and ZnTe are shown below in Fig. 1.4 for comparison.

Since the compounds of interest (CdTe and ZnTe films grown on sapphire) form mainly zinc blende structures, this will be the focus of our discussion. The zinc blende crystal structure consists of two inter-penetrating face-centered cubic lattices, with one lattice being composed of the positive ions, and the other composed of the negative ions (Fig. 1.5) [21][22]. The interatomic separation between adjacent atoms is $\frac{\sqrt{3}}{4}a$, where a is the lattice constant. For bulk CdTe $a = 6.48$ Å, and $a = 6.10$ Å for ZnTe.
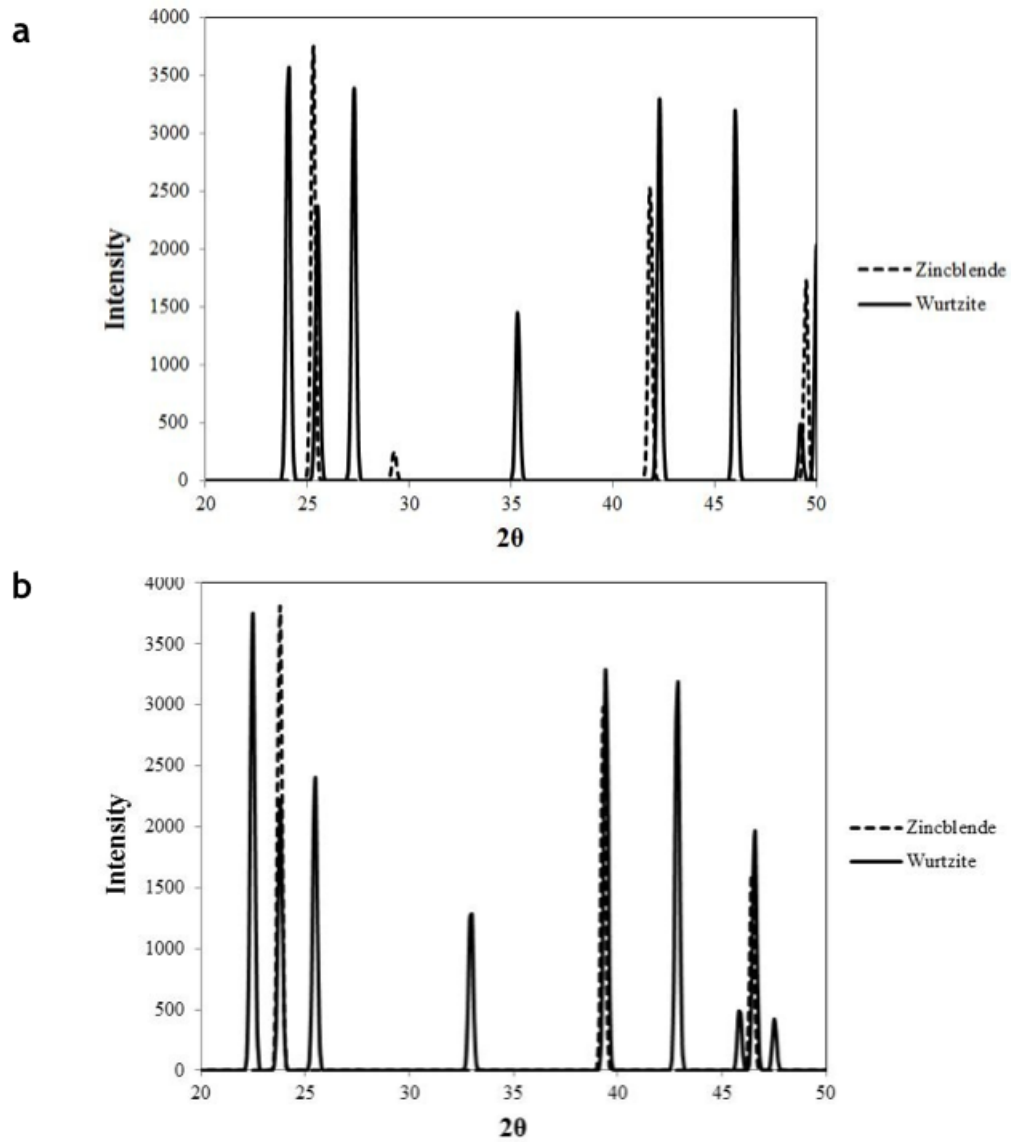
Figure 1.4: Zinc blende and wurtzite powder pattern for a) ZnTe and b) CdTe obtained from the International Crystal Structure Database.
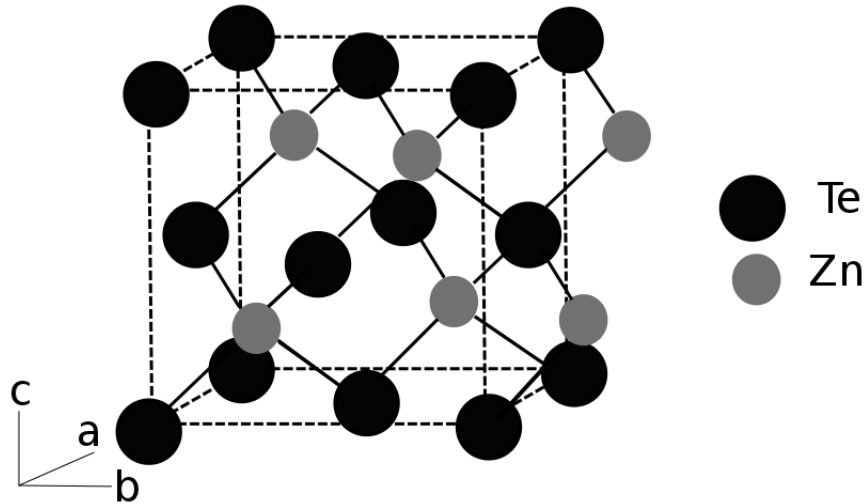
Figure 1.5: Zinc blende crystal structure of CdTe and ZnTe.

The epitaxial growth of CdTe/ZnTe heterostructures (alternating layers of these materials grown on top of each other) will ideally maintain the same crystallographic orientation and lattice structure across the interface so that the boundary does not produce defects that might unexpectedly alter the properties of the material. The interface where the dissimilar materials meet results in a localized strain due to the lattice mismatch between CdTe and ZnTe. For this system, the lattice mismatch is 6.2%. This shifts the lattice constant of both materials in an attempt to minimize the interfacial energy. The amount of shift depends on how much material is on either side of the interface, and how easily these materials tend to deform [23]. Since CdTe has a larger lattice constant than ZnTe, the structure of CdTe at the interface will be compressed, and ZnTe will be stretched.

1.4.2   Optical Properties

The common structure of CdTe and ZnTe contributes to similarities in band structure. Both materials are direct band gap semiconductors, with band gap energies in the visible wavelength range. The band gap of CdTe has been measured to be 1.45 ± 0.10 eV, which corresponds to a red wavelength, and the band gap of ZnTe is 2.20 ± 0.10 eV, corresponding to a green wavelength.

The optical properties of these materials can be tuned by changing their structure or composition. For example, it has been found that the band gap of thin films increases with decreasing film thickness [24]. It has been suggested that the reason for this relationship is that thinner films tend to have a higher defect density, which acts to increase the band gap energy. Another example is the impact that the interface in heterostructures can have on the band structure of a material. When two materials with different band structures meet, there will be an offset in the valence and conduction bands. This can significantly change the optical and electronic properties of the material, and allows for further tailoring for the fabrication of devices [23].

1.5   Motivation

1.5.1   Multilayer Structures

The fabrication of multilayer structures has continued to be of interest since its inception several decades ago, with more diverse materials and fabrication methods becoming available. The layering of various materials to form heterostructures has created countless methods of engineering properties since the materials used, the thickness of each layer, and the effects introduced by the interface can all be tuned to achieve desired results. Similar to the growth of epitaxial films described above, there are three main categories in which a multilayer heterostructure may be grouped: the layered materials can be closely lattice matched with each other and the substrate, or they can be lattice

matched with each other but not the substrate, or the layered materials are not matched with each other and the substrate. Multilayer films with some lattice mismatch can promote interesting effects such as energy level mixing between alternating layers [25].

Multilayer semiconductor films have also received attention because of their potential for band gap engineering. The ability to finely tune optical properties in order to achieve a desired design has been incredibly useful in the development of optoelectronic devices. Because of this, much research has been done on how the band structure of a material may be modified [26]. One method of accomplishing this has been to form multilayer films composed of materials with differing band gaps. Changing parameters, such as the thickness of each layer, the dopant concentration, and the materials used, allows the resulting band gap of the structure to be tuned. This phenomenon has been used to develop novel optoelectronic devices that would not be possible if only a single material were used [26].

CdTe/ZnTe multilayers are strained structures with a tunable band gap in the green region of the visible spectrum, making them desirable for optoelectronic applications. It has been observed that the band gap energy shifts to higher values (i.e closer to the value for bulk ZnTe) as the CdTe layer width is decreased, and that carrier lifetime in these structures is also dependent on the layer widths, demonstrating the customization possibilities of these structures [27][10]. It has also been observed that polycrystalline CdZnTe layers may form from interdiffusion across the CdTe/ZnTe interface when annealed at high temperatures, creating additional opportunities to achieve novel material properties [28]. In addition, the nearly ideal band gap and high absorption coefficient of CdTe makes it a strong candidate for improved solar cell technologies, and layering CdTe with ZnTe is thought to enable the formation of stable ohmic contacts for electronic components [11].

1.5.2   Quantum Wells

A potential application of CdTe/ZnTe heterostructures is that they can be modified to produce quantum wells. These are structures were a narrow band gap material (CdTe) is layered between a wide band gap material (ZnTe). This creates a potential well resulting from the difference in band edges, with the middle layer acting as the well and the outside layers acting as potential barriers (Fig. 1.6) [29]. If the well layer is thin enough that it is on the order of the de Broglie wavelength of the charge carrier (typically a few nm), the energy levels in that layer become quantized and the charge carriers become confined to two-dimensions. The situation is analogous to a particle-in-a-box. Here, the wavefunction for each energy level (indexed N) has solution

$$\psi_N(z) = \sqrt{\frac{2}{a}} sin(\frac{\pi N z}{a}) \tag{1.6}$$

and associated energy

$$E_N = \frac{\pi^2 \hbar^2 N^2}{2ma} \tag{1.7}$$

where a is the length of the well and m is the mass of the confined charge carrier [13].

These structures possess many unique properties because of their quantum confinement. For example, the density of states is modified from the continuous 3D case to a step-like distribution in the confined, 2D case, where each step corresponds to a discrete energy level in the well (Fig. 1.7). If the width of the well is increased, the density of states will begin to resemble the 3D distribution as more steps are compressed in the same energy range [29]. This phenomenon forms the basis of quantum well lasers, which are able to meet the threshold for population inversion at lower energies because of their step-like density of states [13][30].

Changing the width of the well, the materials used, dopant concentrations, and the even the density of wells, provide ways of modifying the properties of
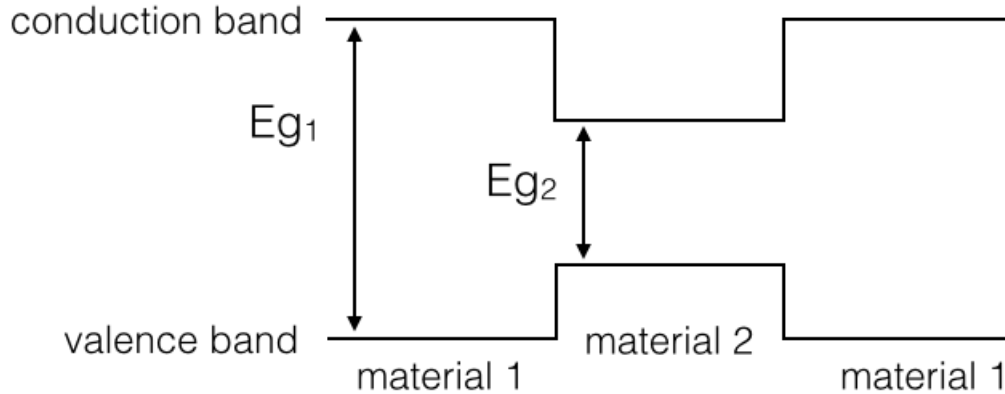
Figure 1.6: Band structure of an ideal quantum well

these structures, allowing them to be tailored to accommodate many different applications. In addtion to lasers, quantum wells are currently used in devices such as high mobility transistors, photodiodes, and optical modulators [13][29].

1.6 Review of Previous Work

1.6.1 Growth of CdTe on Sapphire by Pulsed Laser Deposition

The growth and characterization of CdTe thin films on sapphire has previously been studied in detail [31]. The dissimilar crystal structures and lattice mismatch of 4.2 % makes this an interesting system in the study of heteroepitaxy. Sapphire has a hexagonal crystal structure, with lattice constants a = 4.76 Å and c = 12.99 Å , and is illustrated in Fig.1.8 [32]. In addition, (0001) sapphire substrates have been found to produce nearly single-crystal CdTe epitaxial films, which outperformed several other substrates, including [100] Si, [100] MgO, [110] MgAl$_2$O$_3$, [100] SrTiO$_3$, [110] SrTiO$_3$, [1102] sapphire, [100] yttria-stabilized
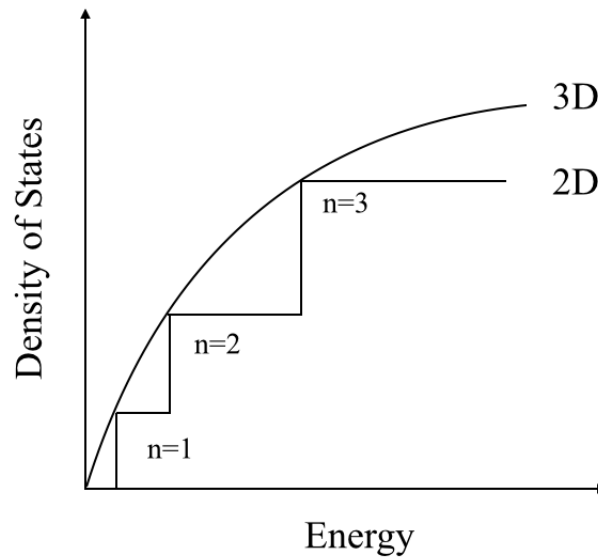
Figure 1.7: Density of states for a 3D material compared to a 2D material, with n indexing the energy level.

zirconia, [001] LaSrGaO$_4$, and [001] ScMgAlO$_4$, determined by X-ray diffraction and atomic force microscopy [33].

C-plane (0001) sapphire is cut so that the surface atoms form a hexagonal arrangement with the long c-axis directed upwards (normal to the surface). The surface is thought to terminate between two layers of Al atoms, possessing three-fold symmetry, in order to preserve charge neutrality. This configuration presents the most favourable option for growing cubic CdTe on sapphire, since the length of the [111] plane contained within the CdTe unit cell, which also possesses a three-fold symmetry, is slightly more than twice the lattice constant of the hexagonal sapphire face [34].

There are two nearly equivalent orientations a three-fold symmetric film may acquire when grown on this surface, and are depicted in Fig. 1.9. These two configurations are 180° rotations of each other about the central (111) axis,
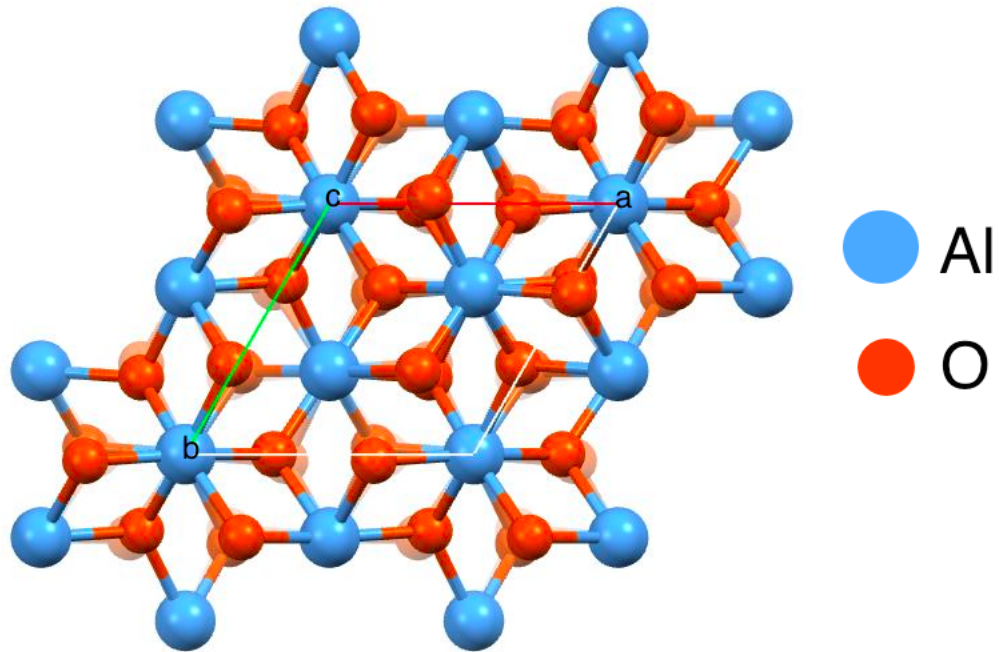
Figure 1.8: The unit cell of sapphire, viewed down the c-axis. Created using Mercury software [1]

.

normal to the surface, and are referred to as a first-order twins. Physically these twins are crystal grains that are atomic mirror images of each other, with the boundary acting as a mirror plane. An additional rotation about one of the other (111) directions (eg. a rotation about the (-111) axis) produces a grain of a different orientation, referred to as a second-order twin. A high quality film will form primarily one domain.

The effect of growth conditions on the resulting quality of CdTe films was also previously studied. The optimization of substrate temperature and plume flux (the rate of materials arriving at the substrate) that yield high quality films was determined using X-ray diffraction, photoluminescence, and photoreflectance spectroscopy techniques. It was found that a substrate temperature of 300° C
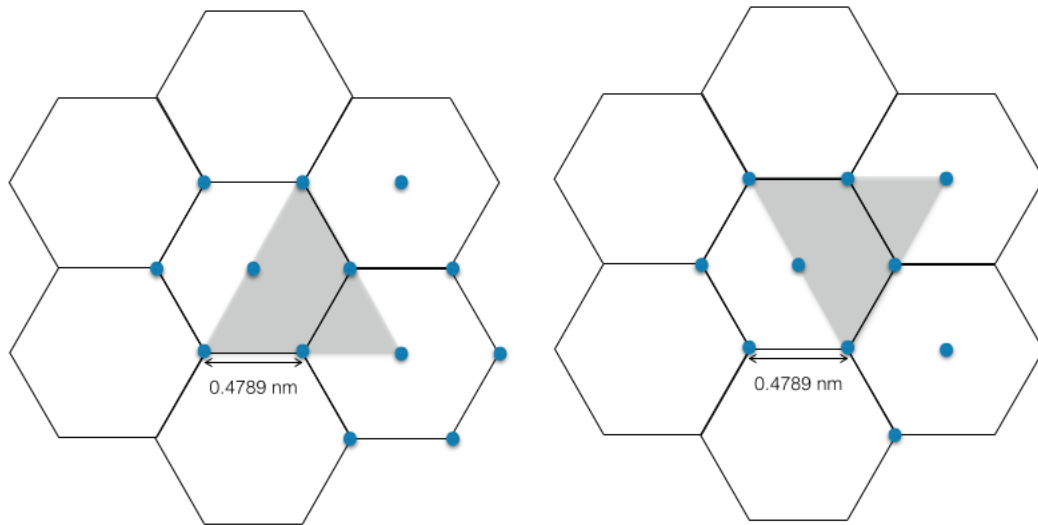
Figure 1.9: Two possible (111) orientations CdTe and ZnTe (gray overlay) may acquire when grown on (0001) sapphire.

provided the best balance between film quality and desorption effects, with a decrease in twin density as temperature increased. Higher quality materials were also obtained at lower flux, with the optimized target-substrate separation being 8 cm, a 0.5 Hz pulse repetition rate, and energy density of 2 J/cm^2 delivered to the target [31].

1.6.2   Lift-off of CdTe films

Nearly single-crystal quality CdTe films can consistently be produced by epitaxial growth on a sapphire substrate. The quality of these materials is much higher than that of CdTe grown with other reported substrates, but is much more expensive, limiting its potential for use in large scale production [33]. The recent discovery that epitaxial CdTe films are able to lift-off of sapphire after growth and be transferred to a carrier bypasses this limitation. This has been successfully accomplished using a variety of carriers, including glass

(transferred by optical cement), copper coated PCB (transferred by solder), and polysulfone. This discovery was exciting for many reasons: The ability to reuse sapphire without the need for intense surface treatments allows for the production of low cost, high quality films, making this system more appealing for industrial applications. In addition, transferring high quality films to a variety of materials that could not other-wise be grown on creates potential for many new applications.

The lift-off of an epitaxial film from its substrate has long been of interest. In 1978, it was shown by Konagai that a GaAs film could be separated from its substrate by etching away an intermediate layer using hydrofluoric acid [35]. Since then, improvements to this procedure have been made, including the use of thinner intermediate layers, less corrosive acids for etching, an extension to II-VI semiconductor films, and the inclusion of a wax capping layer to strain the film relative to the substrate and decrease etching time [36][37]. However, the process developed to remove CdTe films from sapphire has several advantages over these other techniques, including the elimination of extensive chemical treatments and etchants that prevent the substrate from being reused, and requiring much less time to complete (etching can still take several hours) [38][37].

As an example of this process, the transfer of a film from sapphire to polysulfone is described as follows and illustrated in Fig. 1.10. First, a CdTe sample is placed on a hot plate so that the film faces upwards, and a piece of polysulfone cut to approximately the same size is placed on top. The polymer is heated by the hot plate to a temperature above its glass transition point (about 180° C), so that it begins to flow over the film. Using a metal cylinder, the polymer is rolled over the surface of the film to remove any air pockets and ensure good adhesion over the entire surface. The sample is cooled to room temperature so that the melted polymer solidifies. A scalpel and tweezers are used to pry the polymer away from the sapphire so that the two materials separate. Using

this technique, the film is transferred to the polysulfone carrier, leaving a bare sapphire substrate behind.
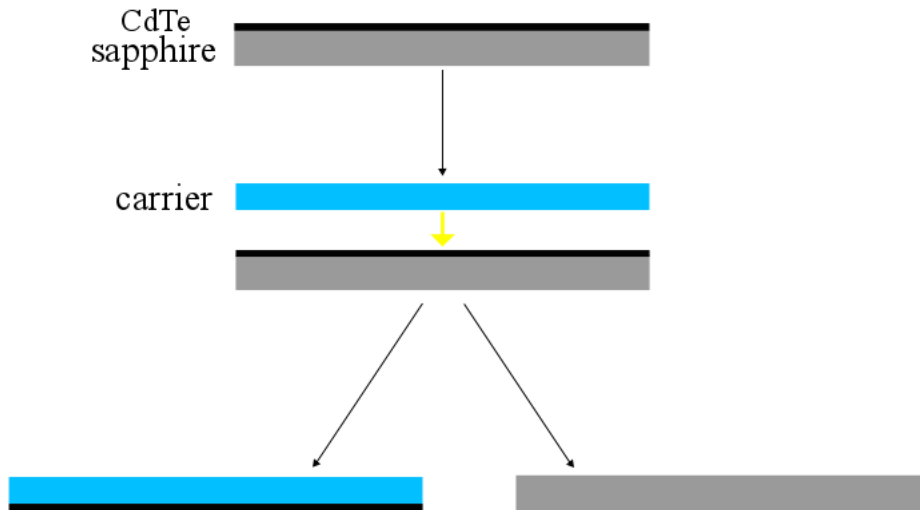
Figure 1.10: Schematic diagram of lift-off procedure used to transfer CdTe from sapphire to polysulfone: a carrier is placed on top of the film and heated so that it melts. Once cooled, the carrier and sapphire are separated, with the film transferring to the carrier.

X-ray diffraction was used to confirm that the quality of the film was not compromised by the lift-off process, and that the remaining sapphire substrate could be reused to grow additional CdTe film of high quality. Photoluminescence of the film before and after lift-off revealed a relaxation of the strain in the lifted-off film, as evidenced by a shift in the photoluminescence peak [31]. The mechanism by which the film becomes detached from the substrate is not well understood, and work is currently being done to further investigate this phenomenon.

Chapter 2

Experimental Techniques

2.1 Pulsed Laser Deposition

2.1.1 Background

Pulsed laser deposition (PLD) is a method commonly used in research to grow epitaxial thin films. In this technique, a high energy laser pulse strikes a target, creating a plume of energetic atoms which condense on a nearby substrate, forming an epitaxial layer in accordance with the substrate's lattice. Additional atoms produce an epitaxial film made up the target material. Advantages over other vapour deposition methods, such as molecular beam epitaxy and chemical vapour deposition, include a roughly equal elemental stoichiometry between the target and film, flexibility in geometry and design due to most components being external to the growth chamber, and applicability to most solid state materials, such as semiconductors, metals, and superconductors [39]. This technique is also useful for the growth of multilayer films, since multiple targets may be rotated in and out of the laser path while under vacuum [40][41].

The physical principles of this technique can be described by a series of light-matter interactions and thermal processes (Fig. 2.1). The first of these occurs when the laser pulse impacts the target. The high energy pulse, with

a wavelength typically in the ultra-violet range, is immediately absorbed by the target and excites electronic transitions in the material. This energy is transferred to the target lattice as heat and propagates to a depth proportional to the inverse of the absorption coefficient, $1/\alpha$, and a radius of $2\sqrt{D\tau}$, where D is the diffusion constant of the target material and τ is the pulse duration. If enough energy is delivered to the lattice, material will be removed in the form of ionized atoms. The energy density required for this depends on the both the target composition and the properties of the laser pulse, such as wavelength and pulse duration [39]. A plume of ionized atoms results, directed towards a crystalline substrate with an angular distribution described by $cos^n\theta$. The exponential variable, n, is controlled by the laser fluence. Since the distribution is typically narrow, material can only be uniformly deposited on small surface areas [39]. This has limited the use of pulsed laser deposition in industrial applications, although improvements have been made (including beam, substrate, and target manipulation during growth) that allow films to be uniformly deposited on wafers up to 200 mm in size [42].
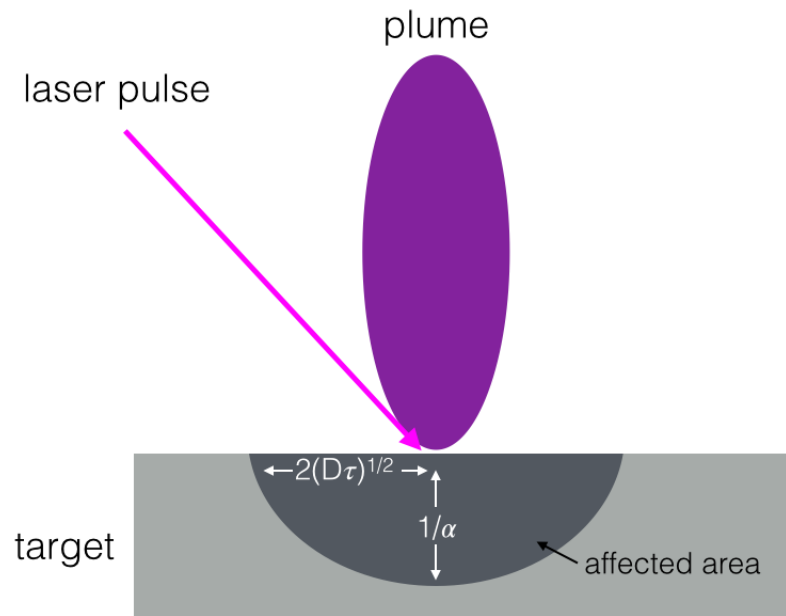
Figure 2.1: The area of a target affected by the impact of a laser pulse and the resulting plume.

Parameters such as substrate temperature, laser power and fluence, pulse repetition frequency, and target-substrate separation, can all be tuned to control the growth of the film at an atomic scale [43]. Care must be taken when setting these parameters, since slight changes can have dramatic impacts on the growth of thin films. For example, if the energy density delivered to the target is high enough to cause the ejection of large clusters of atoms which are deposited on the substrate, the film's growth may be disrupted, causing defects [39]. The pressure inside the growth chamber can also affect the kinetic energies of the ejected atoms as they travel towards the substrate, with energy being lost in collisions. Since a balance of surface energies is crucial to the growth of epitaxial films, the kinetic energies of the adatoms are an important parameter. The substrate temperature also factors into this point. All of these parameters simultaneously dictate the growth conditions and a careful compromise between them is necessary to achieve high quality epitaxy.

2.1.2   Instrumentation

The films in this study were grown using an in-house PLD system, a schematic of which is shown in Fig. 2.2. A GSI Lumonics KrF excimer laser with a wavelength of 248 nm was used. An internal energy monitor within the laser could be set to maintain a constant energy output by automatically adjusting the operating voltage. The voltage required to maintain a particular output energy varied from one growth to another, depending on the age of the laser gas and pressure within the laser cavity. Prior to each growth, the output power of the laser was measured with a Scientech 365 calorimeter and an energy setpoint that would yield 0.8 mJ behind a 15mm by 6.3mm rectangular mask was obtained by manual adjustment. A frequency of 0.5 Hz laser repetition rate was set by an external function generator since 1 Hz is the lowest internally programmable repetition rate. These parameters were chosen based on previous work done with CdTe thin films using this PLD system [31].

A vacuum system connected to the chamber allowed a pressure of 10^{-7} Torr to be maintained during a growth. Once the substrate was mounted to the furnace face and loaded into the chamber, a roughing pump was used to evacuate the chamber to a pressure of approximately 100 Torr. The vacuum was then manually switched over to a turbomolecular pump. A butterfly valve separating the chamber from the vacuum system could then be opened, evacuating the air inside the chamber to a final pressure in the 10^{-7} Torr range. The growth chamber was also equipt with a connection allowing liquid nitrogen to be transferred directly from a tank to a cold finger above the turbomolecular pump, decreasing the time required to reach the appropriate pressure.
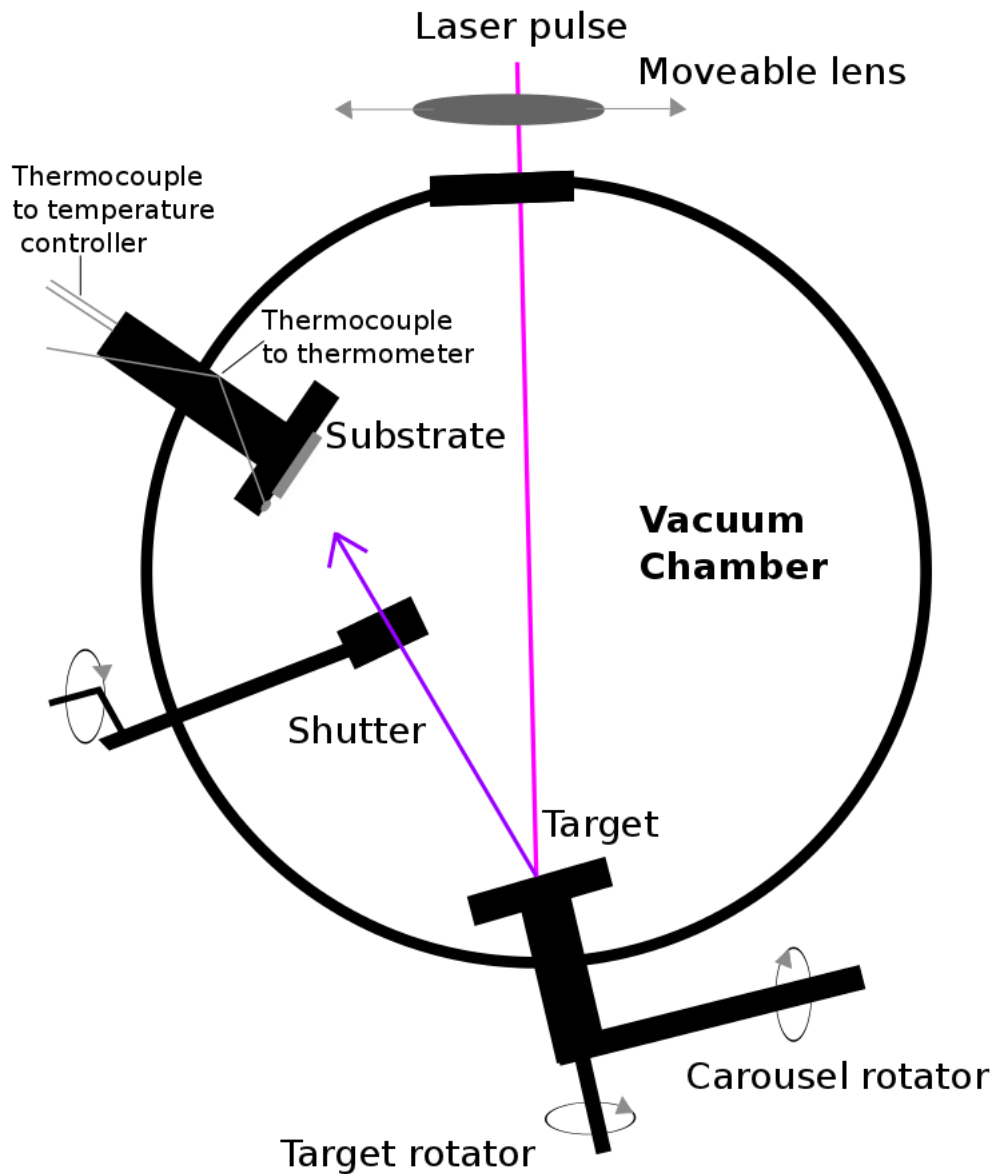
Figure 2.2: Schematic of the PLD system used to grow epitaxial CdTe/ZnTe thin films.

A target rotator and moveable focusing lens were setup to maximize the area of target used during a growth: The rotation of the target created a ring of damage on the target surface, and the changing focusing point from the moving

lens gave the ring a width. A target carousel was used to rotate between target materials without breaking vacuum. This involved the installation of a gear set coupled to an extended rod, held by a metal bracket. The rod could be manually twisted to rotate the target carousel, and the position of each target was marked on the gear set so that targets could be changed and aligned while the chamber remained closed. A moveable shutter situated between the target and substrate allowed for target cleaning without deposition.

A furnace housing an Omega Chromalox cartridge heater was used to heat the substrate to the required growth temperature. Stainless steel ball bearings filled the space around the cartridge to hold it in place and better distribute heat across the furnace face. Two sets of thermocouples allowed the temperature at the heater cartridge and furnace face to be monitored simultaneously. One set of thermocouples was held by the ball bearings against the heater cartridge and connected to an external Omega temperature controller, which automatically cycled the power to the heater by comparing the measured temperature to a programmed set-point temperature. The other set of thermocouples were screwed down to the furnace face, beside the mounted substrate, and connected to an external thermometer to monitor the growth temperature.

2.1.3   Sample Preparation

Contaminants such as dust and other organic materials can disrupt film growth and lead to poor quality results. To remove contaminants from the growth surface, substrates were prepared in the following way. 4" diameter c-plane sapphire wafers purchased from MTI Corp. were diced at McMaster University's Centre for Emerging Device Technology into 12 mm x 12 mm square pieces. The diced wafers were stored in a sealed plastic container inside a desiccator until used. To clean the sapphire substrates, dust caused by the dicing procedure was first removed with nitrogen gas. The substrates were then placed in a sample holder to be cleaned in solvents. The sample holder

was transported to a beaker and acetone was added until the substrates were completely submerged. The beaker was placed in a sonicator set to a tank temperature of 50°C for 30 minutes. The sample holder was then removed from the beaker, and the beaker was emptied and rinsed with acetone. This procedure was repeated using 2-propanol, then methanol, instead of acetone. Lastly, the substrates were removed from the sample holder and dried with nitrogen. They were stored in a covered container cleaned with 2-propanol until used for a growth.

To load the substrate into the vacuum chamber, a mask cut slightly smaller than the dimensions of the substrate was used to secure the substrate to the face of the furnace. Nitrogen was again used to clean the surface of dust before loading the furnace into the growth chamber. Once the furnace was loaded and the pressure had reached 10^{-7} Torr, the substrates were annealed at $400-450$°C for 30 minutes to remove organic contaminants that might still remain on the surface.

The targets were prepared between growths to maintain uniform conditions. As material is ablated, the surface of the target roughens, and was smoothed approximately every four hours of growth time (once for every two growths). This was done by sanding the target inside a clear, plastic bag using emery board. When the damaged area had been sanded away, the target surface would be flat and smooth. Since the target is exposed to contaminants while outside the chamber, the area of the target to be used for growth was also cleaned prior to each growth while under vacuum. The cleaning cycle consisted of laser pulses of 2 Hz repetition for 4 minutes, while rotating the target and moving the focusing lens. A shutter was placed between the target and substrate to prevent the ablated material from being deposited.

The final preparation required prior to growth is to replace the window that allows the laser pulse to enter the growth chamber. Some of the material ablated

from the target is deposited on the window during a growth and eventually builds up enough that it prevents the full power of the laser pulse from passing through. To remove this material, the windows are scrubbed with alumina and 2-propanol using a Kim Wipe until the window appeared clear. The windows are then sonicated in 2-propanol for 45 minutes at a tank temperature 50°C, and dried with nitrogen. The clean windows are stored in a bag, separate from used windows, until needed.

2.2   X-Ray Diffraction

2.2.1   Background

X-Ray diffraction (XRD) is a powerful technique used to characterize the structure of crystalline materials. Information about properties such as lattice parameters, strain, and structural defects (eg. the presence of twins and multiple crystallographic orientations) can all be obtained from XRD analysis. In this technique, a monochromatic beam of x-rays with wavelength λ is incident on a sample. If the angle of incidence θ is such that the reflected beam constructively interferes with other reflections from regularly spaced crystal planes, a diffraction peak is observed. This phenomenon is described by Bragg's law (Fig. 2.3):

$$n\lambda = 2dsin\theta \tag{2.1}$$

where d is the spacing of a set of periodic crystal planes and n is an integer [22]. Each diffraction peak corresponds to a particular set of periodic crystal planes and by sampling various θ, more diffraction peaks are acquired, revealing information about the overall crystal structure of a material.

2.2.2   Instrumentation and Data Collection

2D X-ray diffraction data was collected at the McMaster Analytical X-Ray Diffraction Facility (MAX). A Bruker 3-circle D8 goniometer and Smart6000
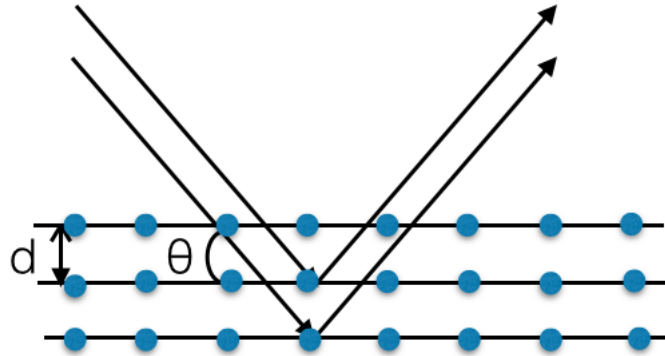
Figure 2.3: Bragg's law. d is the spacing between a regular set of crystal planes, and θ is the angle of incidence of an X-ray beam that results in constructive interference.

CCD area detector were used, with a Rigaku RU200 Cu K$^-\alpha$ rotating anode source with wavelength 1.5406 Å and Goebel cross-coupled parallel focusing mirrors. Fig. 2.4 shows a schematic of the apparatus used. The orientation of a sample is defined by three angles: ϕ specifies the rotation of the sample about its central axis, normal to the surface, ω defines the position of the sample relative to the x-ray beam, and χ represents the tilt of the sample into the beam. The swing angle of the detector is referred to as 2θ and is independent of the sample position.

The data collection method was specified using ApexII software. For most samples, three separate scans were completed, each revealing different information about the structure of the sample. First, a scan of continuous data collection through a full 360° sample rotation was obtained. This scan, called a ϕ360, shows all the Bragg peaks from the sample in the 2θ range scanned on a single frame. These scans are used to clearly show the epitaxial alignment of the sample: Discrete peaks indicate strong epitaxy, while rings of diffuse scattering indicate randomly oriented grains. Broadening of the peaks due to factors such
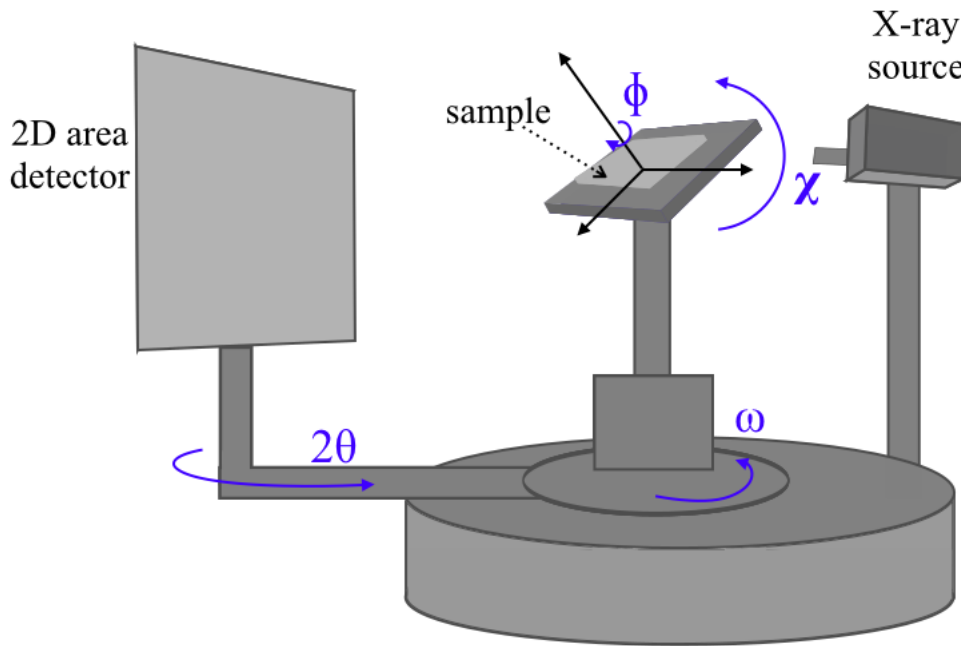
Figure 2.4: Illustration of a typical experimental setup for XRD with the angles of rotation indicated.

as stress can also be qualitatively determined from a $\phi 360$ scan, and multiple sets of peaks from samples composed of more than one crystalline material may also be distinguished. However, since the frame produced by this scan represents the total counts at each 2θ, information about multiple sets of peaks occurring at the same 2θ (i.e. first-order twins) cannot be obtained. Instead, a ϕ scan, consisting of 10 second scans completed every 2° of sample rotation through a full 360°, is completed to probe finer texture detail. This results in a total of 180 frames, with each frame containing information about the sample at a particular ϕ value while $\chi = 54.8104°$ and $\omega = 5°$ are held constant. Information about twinning and other structural defects can be obtained from this scan by stepping through the individual frames to see where each peak contributing to the total count in the $\phi 360$ originates. Lastly, a ω scan is used to sample the angles of incidence near the surface normal. This involves a

collection of 10 second scans at 2 degree intervals around the surface normal. Here, the sample is held at a constant ϕ, 2θ, and χ while ω is varied. This scan focuses on a single peak, corresponding to the set of crystal planes parallel to the surface of the sample, that is passed in and out of it's diffraction condition. This provides information about the alignment of these planes based on the width of the peak, with a broader peak indicating greater misalignment. A comparison of a typical ω scan from ZnTe and CdTe film is shown in Fig. 2.5. The broadening of the peak is determined from the width of the peak, integrated along 2θ.
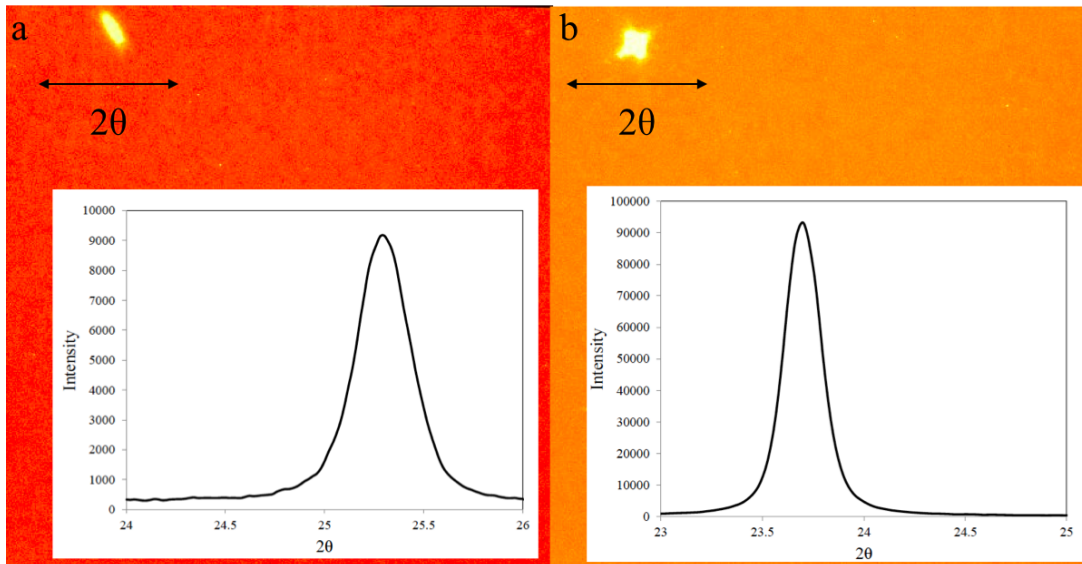
Figure 2.5: Peak obtained from a ω scan for a ZnTe film (a) and a CdTe films (b). The insets show the broadening of the peaks in the 2θ direction.

2.2.3   Texture Analysis

Since most materials are not single-crystal, determining the structure of a sample becomes more difficult. In samples with several grains (crystals with independent orientations within a sample), diffraction will not only depend on the internal structure of the grain, but on the orientation and the boundary

between adjacent grains [44]. In the case of epitaxial growth, a preferred orientation results from the underlying substrate lattice. To determine the preferred orientation and how strongly textured a sample is, a texture analysis can be conducted using XRD data. This analysis is best represented by a pole figure. A schematic of the process used to create a pole figure is depicted in Fig. 2.6. First, XRD is used to create a reciprocal space map of the sample, containing all the detected diffraction peaks. Next, a set of peaks corresponding to a particular set of crystallographic planes is selected (eg. the set of (111) peaks). This subset of peaks is mapped onto a sphere, and then stereographically projected onto a 2D plane. This projection is referred to as a pole figure, and represents the crystallographic orientation of a particular set of crystallographic planes.
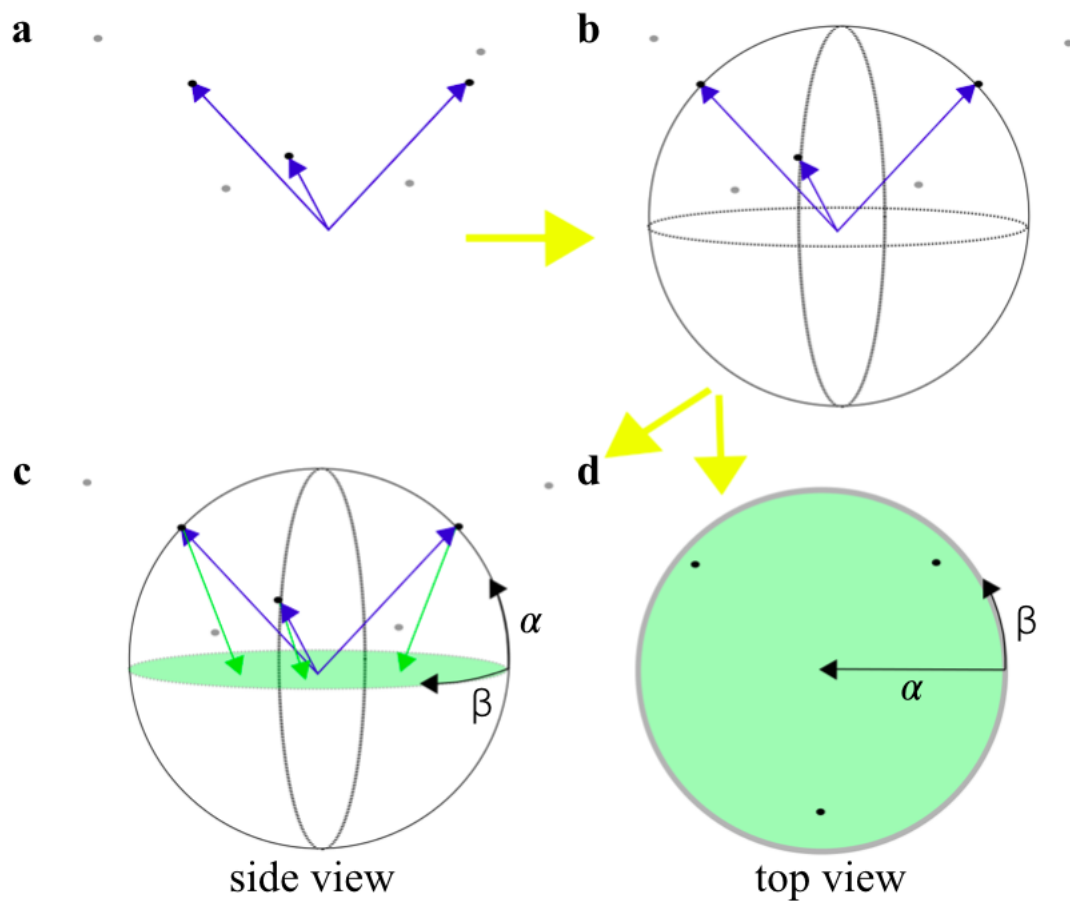
Figure 2.6: Schematic representation of pole figure generation. a) A set of peaks is selected from the reciprocal space map b) The peaks are mapped onto a sphere c) The peaks are stereographically projected onto a 2D plane, viewed from the side. d) Top view of (c) with angles marked for reference.

To perform this analysis, a ϕ scan is completed, resulting in a collection of frames representing information about the sample in 3D reciprocal space. From this set of data, the set of peaks of interest is selected. These peaks can be distinguished from other peaks because they will occur at the same 2θ position in the set of frames. The 2θ width capturing the entire peak is selected and the intensity within this 2θ range is integrated to give a single intensity value at each χ position sampled in the frame. Fig. 2.7 shows how this process is completed in Bruker's General Area Detector Diffraction System (GADDS) software for a single frame. This integration is continued for every frame (180 ϕ
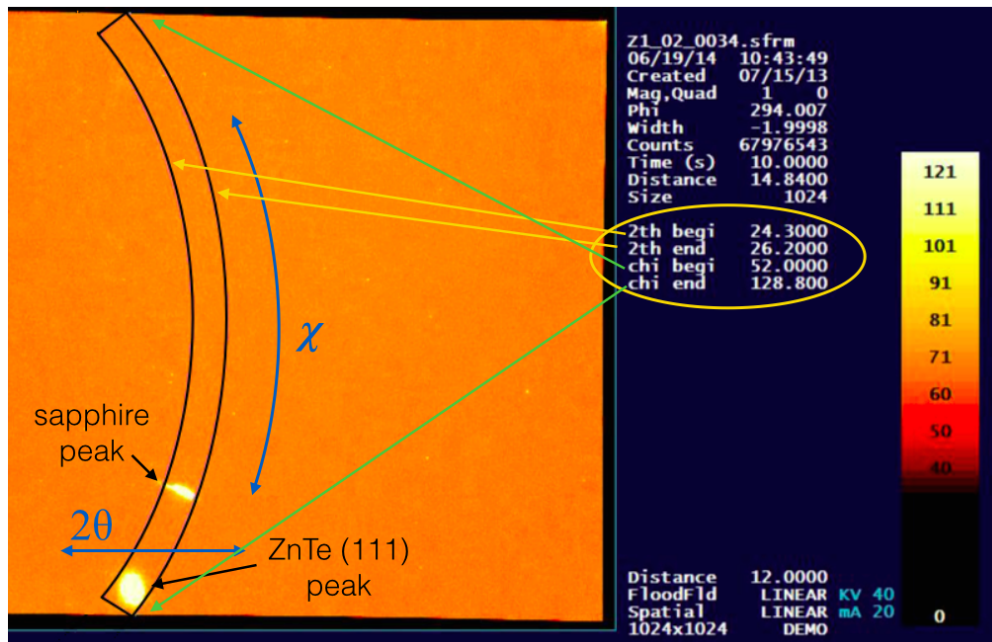
Figure 2.7: GADDS interface showing the integration region used to compile a pole figure. The 2θ and χ directions are shown.

positions sampled) and each frame contributes an intensity that is mapped onto the pole sphere. When complete, each point on the sphere is stereographically projected onto a 2D plane to create the pole figure. Since data is collected every 2°, the pole figure is interpolated to fill in missing regions and create a smooth image. This is done within GADDS by scanning through nearby intensities and choosing a continuous value. A colour scale is automatically generated to

represent the relative intensity at each point on the pole figure.

2.2.3.1   Interpretation

From the pole figure, the texture of a sample is readily obtained. Discrete peaks represent a strongly textured sample, while a ring of diffuse scattering will indicate random grain orientation (i.e. no texture). In addition, the width of the peaks provide important information about the uniformity of the crystal structure. The central peak in the pole figure, corresponding to the direction normal to the sample surface and obtained from the ω scan, has a width associated with plane alignment. If the planes are parallel throughout the sample, the peak will have one value, and no width. However, if the planes are not parallel, the peak will acquire a width associated with the degree of non-uniformity in the plane orientation. Similarly, the in-plane peaks acquire a width if there is a rotation of the plane orientation from one plane relative to another. Additional peaks that are not associated with the selected set of planes may also appear in the pole figure if they are captured by the 2θ integration, such as the sapphire peaks indicated in Fig. 2.7, or if the selected planes possess multiple orientations. An example of this in (111) CdTe is described in the Introduction and Results sections, and manifests itself as two discrete sets of peaks, 180° rotations of each other.

CdTe and ZnTe prefer to grow in the [111] direction on a sapphire substrate. The expected pole figure for the set of 111 planes is depicted in Fig. 2.8. A centre peak results from the planes parallel to the surface of the film, and the other three peaks result from the (-111), (1-11), and (11-1) planes. If a sample is textured, meaning it has a strong preference to grow in the (111) direction, these are the only peaks that will appear in the pole figure. Any additional peaks correspond to additional orientations within the film.

(111) pole figures were created for each sample studied. To accomplish this, Bragg peaks corresponding to the (111) set of planes were first selected. For
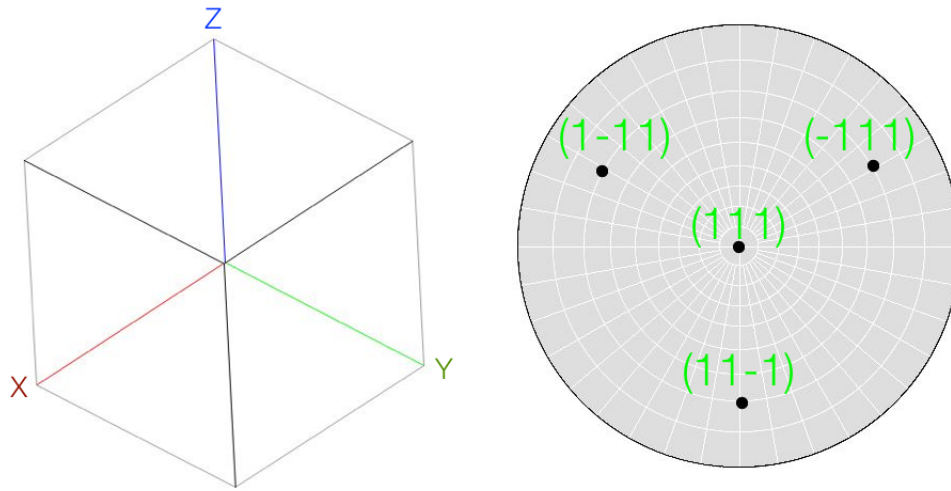
Figure 2.8: Unit cell viewed down the (111) axis (left) and expected (111) pole figure for single crystal CdTe and ZnTe (right).

cubic systems, the 2θ that a d-spacing corresponds to can be calculated using Bragg's law (Equation 1.1) and the relation

$$d = \frac{a}{\sqrt{h^2 + k^2 + l^2}} \tag{2.2}$$

where a is the lattice constant and h, k, l are the Miller indices of the plane of interest. For the (111) planes, the d-spacing can be calculated to be 3.74 Å for CdTe, and 3.89 Å for ZnTe. Using Bragg's law and the known wavelength of Cu K_α line (1.5406 Å), the (111) peaks for CdTe will occur at $2\theta = 23.77°$ and at 25.28° for ZnTe.

2.2.3.2   Relative Intensity Measurements

It is often the case that CdTe films acquire two (111) orientations, resulting in the appearance of multiple sets of peaks in their pole figure. The set of peaks aligning with the sapphire reference peaks are referred to as B peaks, and A peaks when they are misaligned by 60°. The relative intensity of each set can reveal important information about a sample. To determine the intensity of a set of peaks, an integration path and width is specified within GADDS

software to enclose the peaks of interest. Fig. 2.9 shows a screen shot of this procedure for a CdTe sample. The highlighted ring around the outer edge of the pole figure shows the integration range. Peaks belonging to both the A and B type domains are enclosed. A plot of the intensity as a function of the position along the integration path is generated by GADDS. The peaks corresponding to the A and B domains are indicated in the figure. Since the intensity scale is automated and cannot be customized, the generated plot is saved and opened in a plotting program such as Excel or Fityk for further analysis.

Any tilt the sample has when the XRD data was acquired leads to an inconsistent peak intensity in the same set of planes, and so an average intensity for the A set and B set was determined. Comparing the B/(A+B) intensity ratio provides a way of quantifying the fraction of the sample that has the B orientation or A orientation, providing information on the quality of a sample. A high quality film will be single domain, indicated by a B/(A+B) intensity of 0 or 1.

2.2.3.3   Peak Fitting

The 2θ position of the diffraction peaks and their full-width at half maximum (FWHM) can provide important information about the structure of a sample. To obtain these values, the (111) peak was isolated from a ϕ 360 scan (an XRD scan showing all the diffraction peaks collected from a full 360° sample rotation in one frame), as shown in Fig. 2.10. An integration of the intensity across a constant 2θ range was saved as a raw text file and analyzed in Bruker's DIFFRACplus Topas 4.2 software. The data was smoothed prior to analysis to remove any pixels in the background that might affect the fit of the peak. A symmetric pseudo-Voight function (a combination of a Gaussian and Lorentzian profile) was used to fit the peaks and obtain the peak position, FWHM, and associated errors. An additional error accounting for potential sample misalignment was also included. This was done by mounting a sample four times and collecting
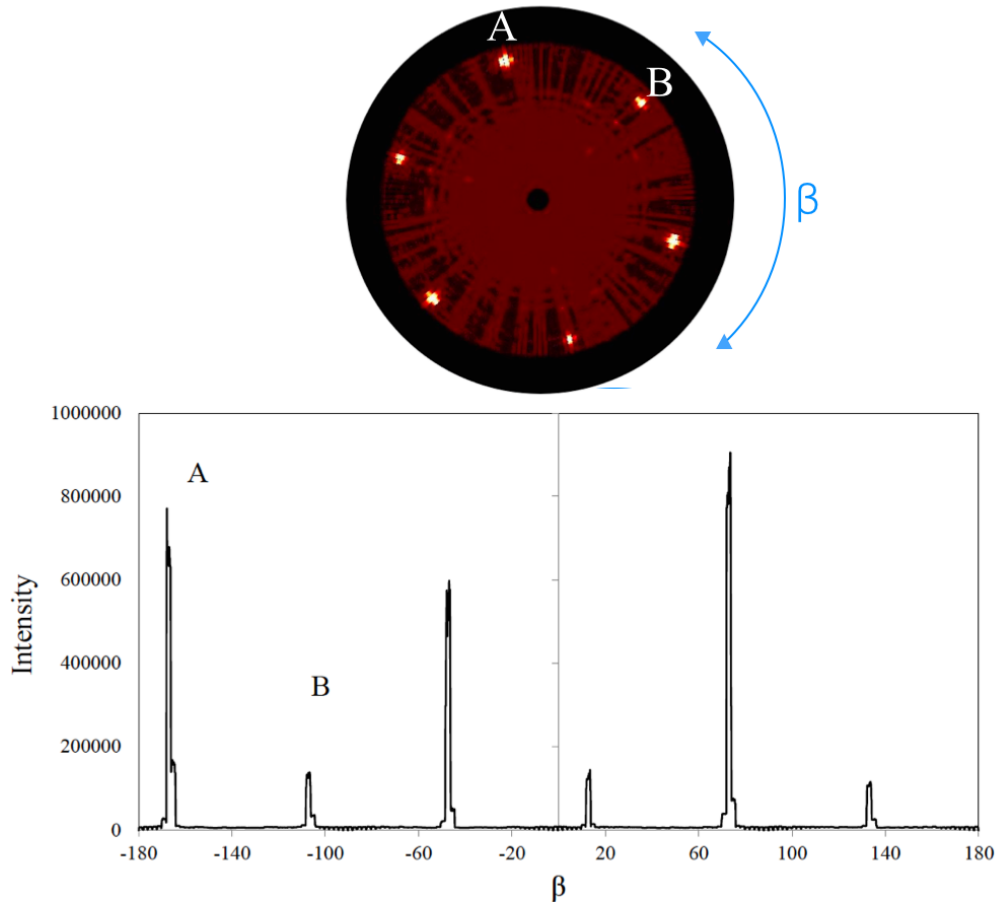
Figure 2.9: A pole figure of a CdTe sample (top) is used to compare the relative intensity of peaks corresponding to A and B domains within the sample (bottom).

a $\phi360$ scan for each trial, then using Topas to fit the (111) peaks so that an average peak position and FWHM could be found. The largest deviation from the average in the set of measurements was taken to be the error associated with sample misalignment, with the total error in the peak parameters being the sum of the misalignment error and the program fitting error.
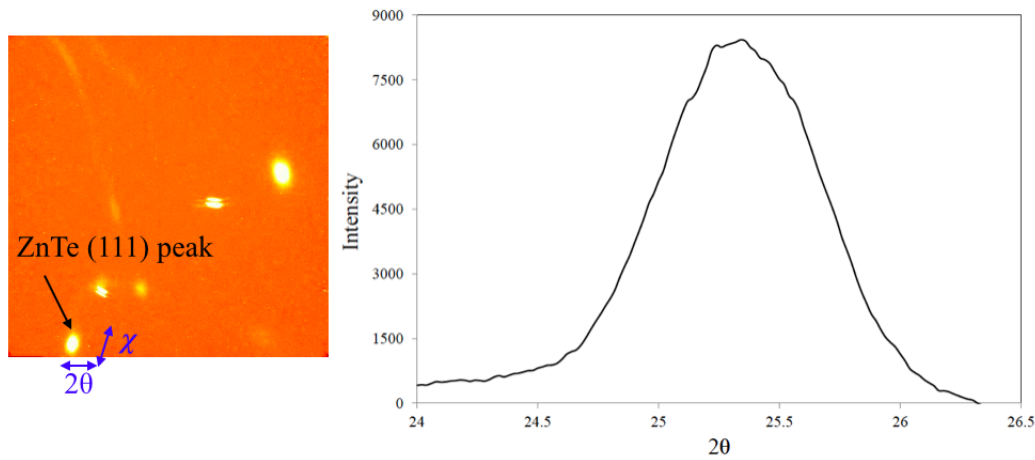
Figure 2.10: A $\phi360$ scan of a ZnTe sample (left) is used to obtain the intensity of the (111) peak along 2θ (right). The data is further analyzed to find the centre position and FWHM values.

2.3 UV-Vis Spectroscopy

2.3.0.4 Background

UV-Vis spectroscopy is a technique commonly used to characterize the optical properties of materials. A range of ultraviolet and visible wavelengths are passed through a sample and the difference in the intensity between the incident and transmitted beams is used to determine the absorbance of the sample at each wavelength.

Photons of a particular wavelength carry a specific amount of energy:

$$E = hc/\lambda \tag{2.3}$$

If the amount of energy carried by the photon is enough to allow an electronic excitation within the sample, the photon will be absorbed. An absorption spectrum can then be used to reveal information about the electronic properties of a sample.

The band gap of a semiconductor is the energy difference between the valence and conduction bands and is the smallest amount of energy required to produce an electronic excitation. UV-Vis spectroscopy can be used to determine the band gap by identifying the wavelength or energy at which the onset of absorption occurs. For crystalline semiconductors, the band gap energy E_g is related to the absorption coefficient $\alpha(\nu)$:

$$\alpha(\nu)h\nu = B(h\nu - E_g)^m \tag{2.4}$$

where B is a constant, $h\nu$ is the incident photon energy, and m is an index that depends on the electronic transition. The absorption coefficient represents the rate at which light intensity decreases along its propagation path through a material, and can be expressed according to Beer's law as

$$\alpha(\nu) = \frac{2.303 \times A(\lambda)}{d} \tag{2.5}$$

where d is the thickness of the film and A(λ) is the film absorbance [45][46]. By combining equations (2.4) and (2.5), and rewriting $h\nu$ in terms of λ (Equation 2.3), we find

$$A(\lambda) = C\lambda(\frac{1}{\lambda} - \frac{1}{\lambda_g})^m \tag{2.6}$$

where C is a constant, containing the film thickness, d. A(λ) is the value measured by the UV-Vis spectrometer, and so the band gap can be determined by plotting $(\frac{A(\lambda)}{\lambda})^{1/m}$ against $1/\lambda$ and extrapolating the linear region to zero absorption [46]. The energy at which the extrapolation crosses the x-axis is taken as the band gap energy. This type of plot is commonly used for determining the band gap of a material, and is called a Tauc plot [24]. For most direct transitions in crystalline semiconductors, m = 1/2 [47]. The Tauc method is named for it's creator, who first developed this procedure to describe the absorption edge in germanium and silicon in 1968 [48]. These plots are often reported in terms of energy instead of wavelength, and use of equation 2.3 will show that the band gap can also be obtained by this method from a plot of $(\alpha h\nu)^2$ vs $h\nu$. An example of this process, applied to a ZnTe thin film by Ghosh, B. et al., is shown in Fig. 2.11.
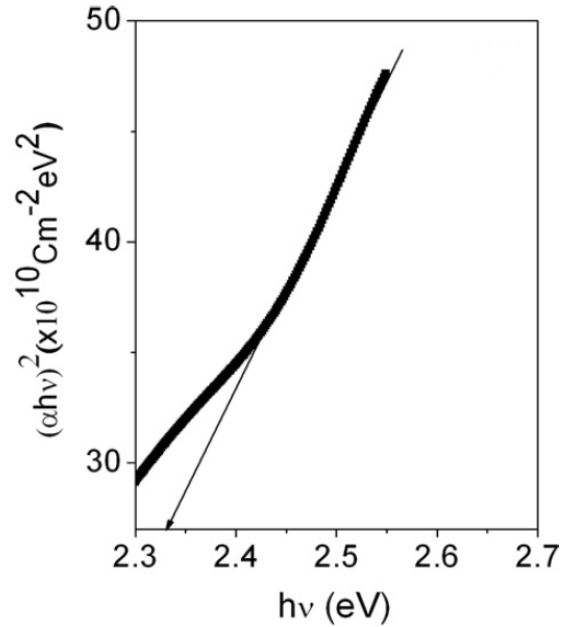
Figure 2.11: The Tauc method applied to a ZnTe film to determine the band gap energy (Reused from [2] with permission from Elsevier).

2.3.0.5 Instrumentation and Data Collection

Absorbance spectra for various samples were collected using a Varian Cary 50 UV-Vis spectrometer. A Xenon lamp produces an intermittent beam of radiation which is only activated at the time a data point is collected. The beam is passed through a beam splitter and monochromator, then focused onto the sample. A photomultiplier detector measures the intensity of the transmitted beam and generates an absorbance vs wavelength spectrum based on the difference in the intensity of the incident and transmitted light beams [49]. A homemade sample holder was used to support the samples so that light could pass through the centre and be collected by the detector. A wavelength range of 1100-190 nm was scanned at the slowest scan speed set by the instrument to generate the most data points, allowing smooth absorption curves to be generated.

2.3.0.6   Band gap Determination

Data collected from the Varian Cary 50 UV-Vis spectrometer was saved in a spreadsheet and analyzed in Microsoft Excel and xmgrace software. The full Tauc curves were plotted and then zoomed in to focus on the absorption edge. Points within the linear region were selected and fit to a linear trendline. The trendline was then extrapolated to $(\alpha h\nu)^2 = 0$ and the band gap energy was extracted from the line equation. A standard error for band gap was determined using errors for the slope and intercept generated from the xmgrace analysis.

2.4   Additional Characterization Techniques

2.4.1   Electron Microscopy and Spectroscopy

2.4.1.1   Background

The interaction between electrons and matter has been used to probe the structure of materials for many years and is employed in a variety of characterization techniques. When a beam of electrons is incident on a sample, excitations result in the emission of photons and electrons from various processes (Fig. 2.12). Depending on the energy of the incident beam and the composition of the sample, the electrons are able to penetrate into the sample before experiencing interactions, allowing information from various depths within the sample to be gained [50]. Secondary electrons, which are emitted from the valence shell of an atom, have relatively low energy and are reabsorbed by the sample unless they are created within a few nanometers of the surface. Backscattered electrons are those elastically scattered from the sample and posses energies higher than secondary electrons since there is little energy lost in the interaction. Because of this, they may originate from deeper in the sample and carry information about it's interior. Backscattered electrons can also produce secondary electrons through collisions within the sample [3]. If a core shell electron is removed from an atom, an outer shell electron will replace it, causing the release of an Auger

electron. These electrons have energies characteristic of the atom they originate from and so carry information about the sample's composition [51]. In addition, some electrons may be transmitted through the sample, experiencing elastic and inelastic scattering interactions. Characteristic X-rays and other photons may also be emitted as a result of high energy interactions [3]. A comparison of the energies associated with these processes is depicted in Fig. 2.13.
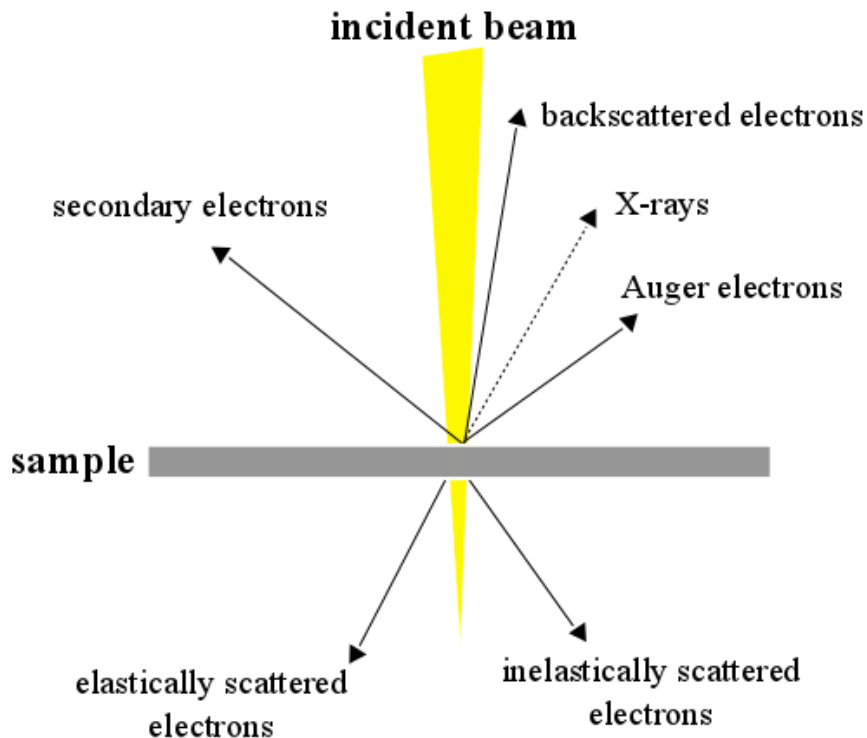
Figure 2.12: Effects of the interaction between a beam of electrons and a sample.

2.4.1.2 Transmission Electron Microscopy and Electron Energy-Loss Spectroscopy

One of the techniques based on these principles is transmission electron microscopy (TEM). In this technique, a sample is thinned to 10-100 nm thickness so that electrons are able to pass through [52]. A beam of electrons interacts
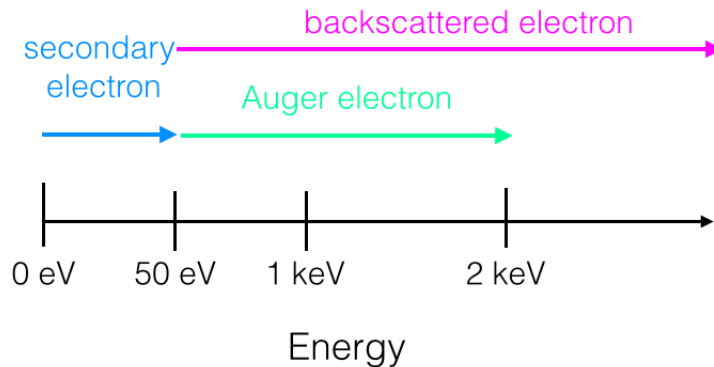
Figure 2.13: Relative energies of electrons emitted from a sample [3].

with the sample via scattering mechanisms and the intensity distribution of the transmitted beam is collected by a series of lenses and focused onto a fluorescent screen [53]. The structure of the sample can be determined from the image by identifying differences in contrast. Atoms with a higher atomic number have more electrons to scatter the incident beam and so less intensity is transmitted through the sample, resulting in darker areas in the image. In contrast, incident electrons are able to more easily pass through atoms with fewer electrons, and so these appear brighter. Atomic resolution (on the scale of 0.1 nm) is possible using TEM since the electrons used to probe the sample have high energies, typically several hundred keV, with a wavelength shorter than the interatomic distances [54].

Scanning transmission electron microscopy (STEM) is a very similar technique, but differs from TEM in the image formation process. In STEM, the electron beam is narrowed to a small spot and rastered across the sample to build an image, as opposed to immediately creating a complete image in TEM where a broader beam is used to sample a greater area at once. STEM images can be collected in bright field or dark field, referring to whether the detector includes the transmitted beam (bright field), or excludes the transmitted beam (dark field) [55]. In bright field, atoms that scatter more of the electron beam

appear darker, and atoms that scatter less of the beam appear brighter. The opposite distinction applies to dark field images.

Electron energy-loss spectroscopy (EELS) is a technique used to characterize the elemental composition of a sample. EELS is conducted within a TEM instrument and uses a low energy beam of electrons to interact with the electrons in a sample, resulting in inelastic scattering. The transmitted beam of electrons are collected in a spectrometer that separates the various kinetic energies of the scattered electrons and determines how much energy was lost in the interaction with the sample. The loses are characteristic of the scattering atom, and can be used to identify the relative amounts of each element present in the sample [56].

2.4.1.3   Auger Electron Spectroscopy

Auger electron spectroscopy (AES) can be used to determine the elemental composition of a sample. A high energy beam of electrons (typically 2-10 keV) is used to remove core electrons from the atoms in a sample [57]. An electron from a higher energy orbital replaces the core electron and an Auger electron, with an energy characteristic to the type of atom it originated from, is released to conserve momentum [51]. The emitted Auger electrons are detected and the measured energy is used to create an elemental profile. Since these electrons have relatively low energy, only those emitted at the surface of the sample are detected [50].

This technique can be combined with ion sputtering to produce an elemental depth profile through a sample. To accomplish this, a beam of high energy ions is used to remove material from the sample. An etching time is specified and an AES measurement is made after each interval [57].

2.4.1.4 Scanning Electron Microscopy

One of the most widely used surface characterization techniques is scanning electron microscopy. Secondary electron imaging is most commonly used since the low energy electrons carry information originating only from the surface of the sample [17]. A detector with an applied bias is used to attract the low energy secondary electrons emitted from the sample as the incident beam is rastered across the surface. The detected energies are converted into photons by a scintillator before entering a photomultiplier tube that ultimately converts these back into electrical signals so that they may be displayed on a screen, producing an image of the sample's topography. A SEM image shows the contrast between regions of high and low intensity, corresponding to regions where the secondary electrons were able to reach the detector (bright areas), or were obstructed (dark areas). In addition, materials with a higher atomic number have a higher density of electrons that interact with the primary beam, resulting in the emission of more secondary electrons. Because of this, brighter areas can also correspond to regions of the sample composed of heavier elements, and darker regions correspond to lighter elements [3]. The resolution of SEM is on the order of 5 nm [54].

Use of this technique can become problematic when attempting to image non-conductive samples. In this case, the incident beam of electrons is not easily conducted away from the surface and charge accumulates instead. This effect is referred to as charging, and repels the electron beam being scattered to the detector, resulting in a very bright image lacking features. Non-conductive samples can still be imaged with some success if the proper preparations are made. This may involve coating the surface in a thin conductive layer, and creating conductive contacts to the metal sample stub.

2.4.2 Atomic Force Microscopy

Atomic force microscopy is a surface characterization technique that uses the interaction between a very sharp tip and a sample to probe the structure of the sample's surface. A schematic of how this is accomplished is shown in Fig. 2.14. The tip, located at the end of a cantilever, is held over the sample. The cantilever is deflected as the tip moves along the surface of a sample, or a sample is moved under the tip. To monitor this movement, a feedback mechanism, such as a laser aligned with the cantilever and a photodiode, is used to detect the deflection. This signal is sent to a computer that then creates an image of the sample topography. Advantages to this technique over other surface characterization tools, such as SEM, are that very little sample preparation is required, measurements are not performed under vacuum, and the sample does not need to be conductive to acquire high resolution images. The height resolution of an AFM is comparable to TEM (around 0.1 nm) [54].
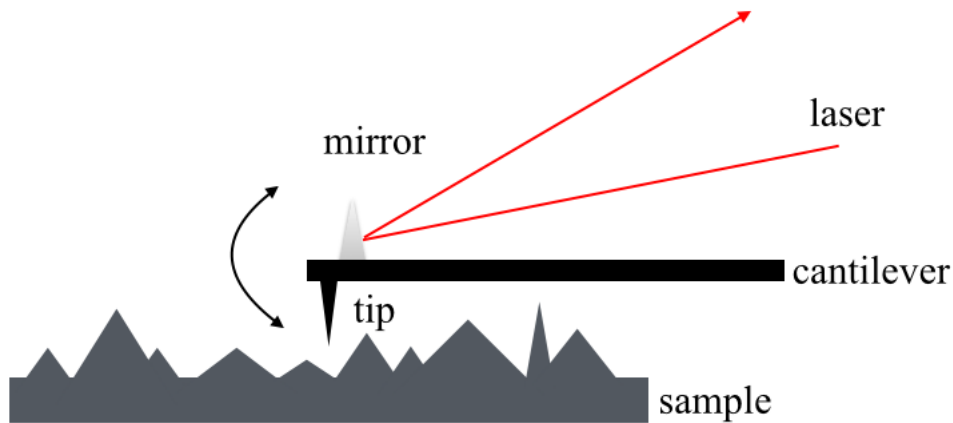
Figure 2.14: Illustration of an AFM topology scan. A feedback mechanism is used to monitor the interaction between a tip and the sample.

There are three modes in which the AFM can collect data: contact mode, non-contact mode, and tapping mode. The contact and non-contact modes can

be further categorized as constant force or constant height mode. In the first case, the force between the tip and the sample is held constant so that the cantilever must move upwards when it encounters an elevation in the sample surface, and downwards when it encounters a depression. In constant height mode, the cantilever is held at a constant height above the sample and detects changes in the force as the topography of the sample brings the sample closer to the tip, or further away [58]. In contact mode, the tip is held a few angstroms above the sample surface so that it is effectively in contact with the sample. Non-contact mode differs in that the tip is oscillated several 10-100 angstroms above the surface of the sample so that it never makes contact. The oscillation frequency and amplitude of the tip changes as it interacts with the sample, and these changes are used to produce a map of the sample's topography. Tapping mode (also known as intermittent-contact mode) is somewhat intermediate. Here, the tip is oscillated, similar to non-contact mode, but is closer to the surface so that the lowest amplitude in its oscillation brings it in contact with the sample [54][59].

Chapter 3

Results and Discussion

3.1 Growth of Single-layer CdTe and ZnTe

3.1.1 Structural Comparison

Epitaxial CdTe and ZnTe thin films grown on sapphire substrates are an unusual system because of the significant differences in the crystal structure of these materials. These semiconductors have a cubic structure with lattice constants a = 6.10 Å and a = 6.48 Å for ZnTe and CdTe respectively, while sapphire has a hexagonal structure with lattice constants a = 4.76 Å and c = 12.99 Å [2][32]. Epitaxial growth depends on a symmetry match between the film and substrate, and so this pairing may at first seem a poor choice. However, despite these striking differences, high crystal quality can result from growth on a sapphire substrate since only the atoms at the interface interact, and so only the symmetry at the surface of these materials are relevant. C-plane sapphire has a hexagonal arrangement of surface atoms, and (111) CdTe and ZnTe also have a hexagonal arrangement of atoms, but possess a three-fold symmetric surface because the two atomic species (i.e Cd and Te or Zn and Te) create unequivalent sites.

As stated in the introduction, there are two possible orientations a (111) CdTe or ZnTe film may acquire when grown on (0001) sapphire. The six-fold symmetry of sapphire is reduced to a three-fold symmetry if the environment created by atoms near the surface are considered. These atoms distinguish two unequivalent sites. The situation then changes to the growth of a three-fold symmetric film on a three-fold symmetric substrate. There is only one orientation that will allow this, but because the two sapphire surface sites differ only slightly, the growth of two film orientations is still possible. An XRD texture analysis can be used to distinguish the two possible (111) orientations. Single-crystal sapphire substrates produce high intensity diffraction peaks that are captured in the (111) pole figure of the film. By comparing the position of the film peaks to the sapphire peaks, which consistently appear at the same position for all samples, the two (111) film orientations can be differentiated. The orientation that results in the film peaks being offset from the sapphire peaks by 60° will be referred to as A domain, and the B domain when they align (Fig. 3.1)
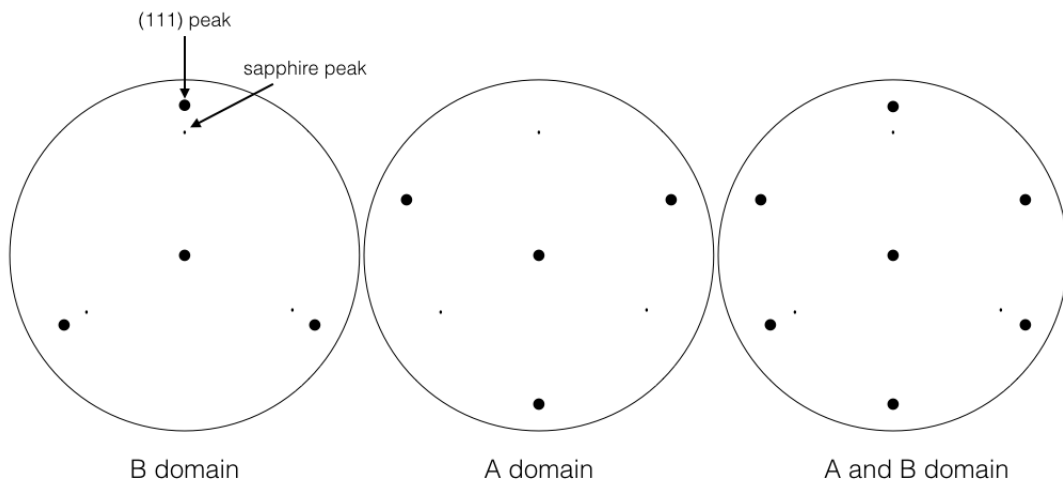
Figure 3.1: Pole figures corresponding to A and B domain growth. Both sets of peaks are present in films with both domains.

3.1.1.1   Correlation Between CdTe Growth Parameters and Crystal Quality

Before beginning the study of ZnTe film growth by pulsed laser deposition, a detailed analysis of previous work done on CdTe films was conducted. This involved analysing XRD data collected for over 100 films grown under various conditions and attempting to find correlations between particular growth parameters (eg. temperature, pressure, etc.) and high quality samples. CdTe and ZnTe are similar in terms of their structure and properties, so this review served as a good starting point for the study of ZnTe.

Most CdTe films analyzed possessed both A and B domains, as evidenced by both sets of peaks in the (111) pole figure. A ratio of the B/(A+B) peak intensity was calculated in order to quantitatively compare the quality of one film to another. If B/(A+B) = 1, only the B domain is present in the film, and if B/(A+B) = 0, only the A domain is present. The highest quality films would have only one domain, corresponding to these two extremes, however most CdTe films fell somewhere in between. The results from this study did not identify any correlation between high quality films and a particular set of growth parameters, suggesting that a more complicated combination of multiple parameters is responsible for the production of consistently high quality materials. Fig. 3.2 shows two CdTe films grown under the same conditions (substrate temperature of 300° C, a pressure of 10^{-7} Torr, pulse repetition rate of 0.5 Hz with a laser power of 80 mJ, and a deposition time of 120 minutes) with varying results in their crystal quality.

3.1.1.2   Dependence of ZnTe Film Structure on Growth Temperature

It was then decided to proceed with the growth of ZnTe using the optimized parameters found in previous studies of CdTe grown on sapphire. These parameters were: a substrate temperature of 300° C, a laser energy of 80 mJ measured
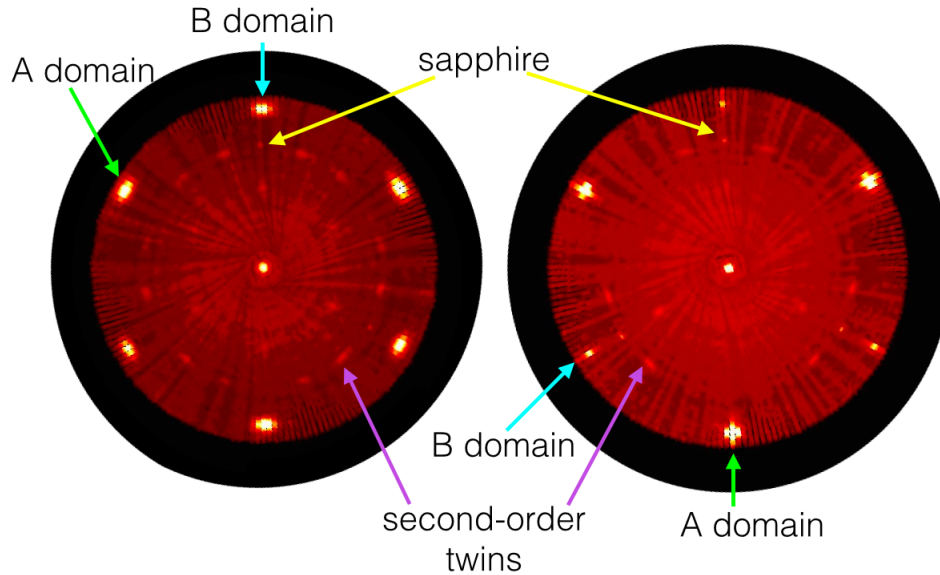
Figure 3.2: (111) pole figures for CdTe films grown under the same conditions. The quality of the films differ significantly, but both A and B domains are present in both.

behind the mask, a repetition rate of 0.5 Hz, a growth time of 120 minutes, and a pressure in the range of 10^{-7} Torr. A 1" diameter ZnTe pressed powder target purchased from 5N Plus was used, and MTI Corp. c-plane (0001) sapphire wafers diced into 12 mm by 12 mm squares were prepared as a substrate.

XRD texture analysis was completed at the McMaster Analytical X-ray (MAX) Diffraction Facility. The resulting (111) pole figure is shown in Fig. 3.4 below. It is immediately obvious that although ZnTe and CdTe have a similar structure, they interact with the sapphire surface differently and their growth is not equivalent. A comparison of the pole figures for each of these materials is shown in Fig. 3.3. CdTe films on sapphire were found to have predominately A domains, with some amount of B domains and second-order twins in almost all cases, while ZnTe films on sapphire had only B domains (i.e. no A domains).
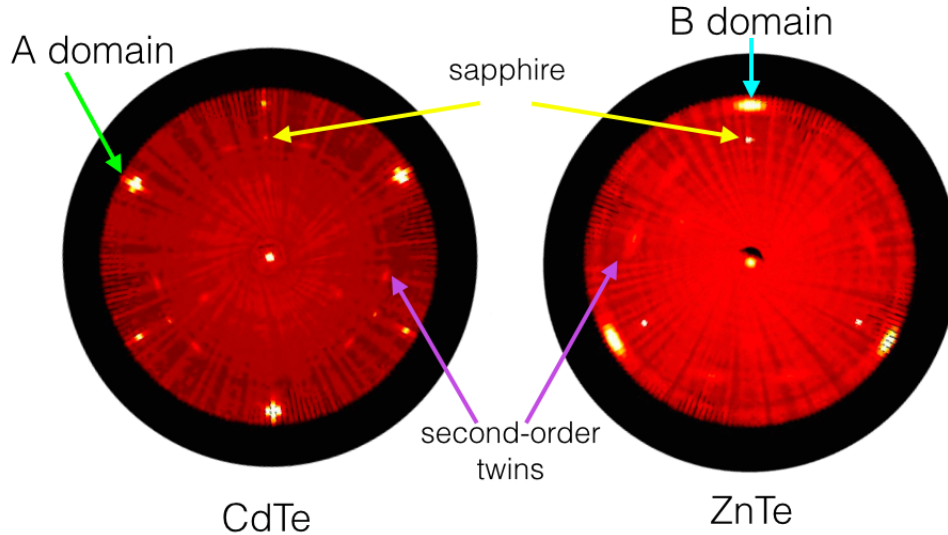
Figure 3.3: (111) pole figures for CdTe and ZnTe grown on sapphire. CdTe films have predominantly A domains, while ZnTe films have only B domains.

To investigate the growth behaviour further, additional ZnTe films were grown at various temperatures between $315 - 420°$ C, all with the same laser settings and pressure range, and with the same preparation and cleaning procedure. Higher growth temperatures were expected to result in higher quality films, since the diffusion energy of adatoms increases with temperature (Equation 1.3), allowing the minimum energy configuration of surface atoms to be established. Fig. 3.4 shows a summary of the pole figures obtained from XRD texture analysis for each of these films.

Similar to the growth at $300°$ C, only B domains were observed, with no A domains, but with some second-order twinning in each of these films. A second-order twin density for each film was calculated, using a similar procedure to that previously used to calculate the B/(A+B) intensity ratio for CdTe films, to quantitatively compare film quality. Here, C/(B+C) is calculated, with B still corresponding to the maximum (111) ZnTe B peak intensity, and C referring to the maximum intensity of the second-order twin peaks. Since the second-order twin peaks had a weak signal and the sapphire peaks dominated

the integrated intensity, the second-order twins were pulled out the background noise by separating the data into thirds (which are symmetric portions of the pole figure), and summing the intensities at symmetric points. The (111) film peak intensities for this ratio were obtained in the same way for consistency. The maximum fluctuations in the background data were used to provide a relative error for these calculations.
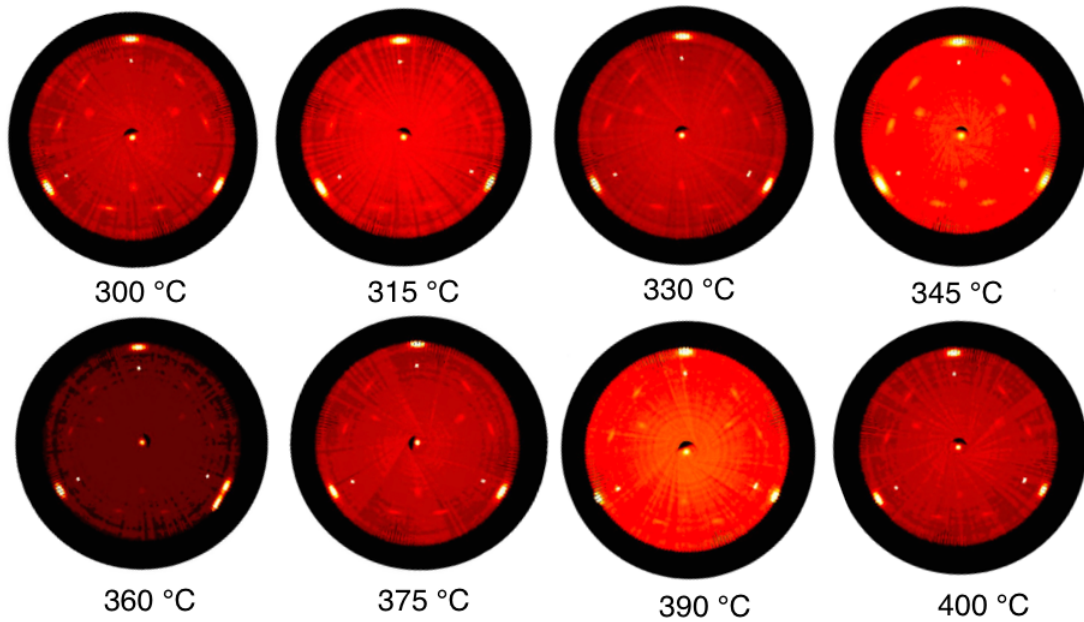
Figure 3.4: (111) pole figures for ZnTe films grown at various substrate temperatures.

As the growth temperature increased, the second-order twin density in the films decreased (Fig. 3.5). Second-order twins are low energy defects and are common in epitaxial films of II-VI semiconductors [60]. The probability that an adsorbed atom moves to a new site on the underlying lattice per unit time is related to temperature and given by Equation 1.3 in the introduction. As temperature increases, the probability of diffusion increases, allowing the adatoms to move about the surface such that they minimize the surface energy.
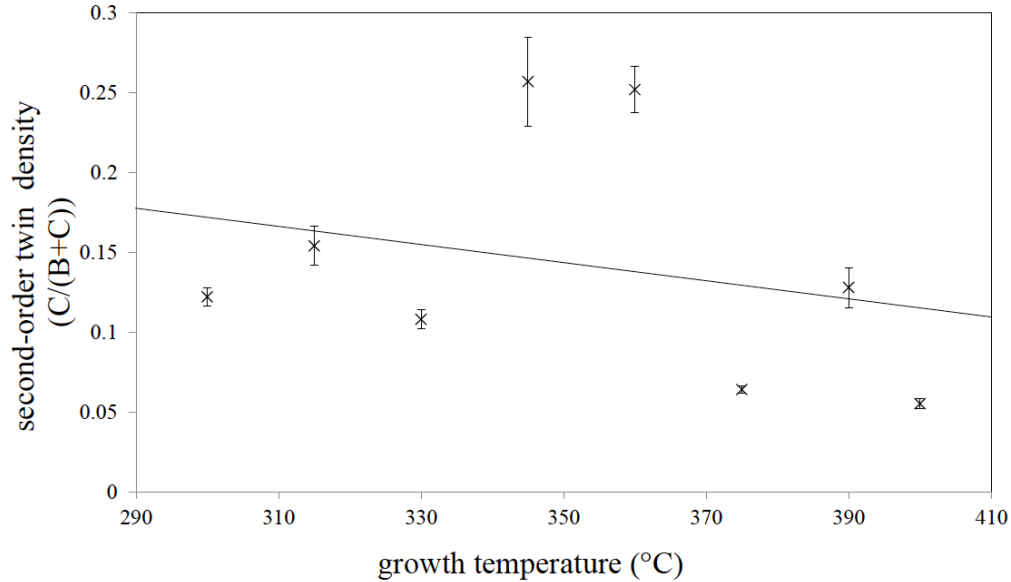
Figure 3.5: Second-order twin density in ZnTe films grown at various temperatures.

However, twinning was never completely quenched, even at temperatures high enough that ZnTe stopped adhering to sapphire long enough to nucleate film growth.

The 2θ position of the (111) peak was found to be between $25.3 - 25.6°$ at all growth temperatures. Using Bragg's law (Equation 2.1), the corresponding (111) d-spacing for the ZnTe films was determined to be 3.48-3.52 Å. The lattice constant was then calculated using Equation 2.2 and found to be 6.02-6.09 Å. This is very close to the value of 6.10 Å reported in the literature for ZnTe, showing that although the interface is strained due to the lattice mismatch, the films assume a relaxed structure throughout their growth and can be classified overall as strain-relaxed.

The width of the (111) film peaks can also reveal information about the structure of thin films. The peak corresponding to the direction normal to the film surface (in the centre of the pole figure) has a width associated

with misalignment in (111) set of planes, with a wider peak indicating more misalignment. Within each plane, there are three other (111) directions: (-111), (1-11) and (11-1), and the width of these peaks are associated with in-plane misalignment, usually resulting from strain. The full-width at half maximum (FWHM) of these peaks were calculated and compared for each ZnTe film grown at $300 - 400°$ C. The results of this analysis are shown in Fig.3.7. No correlation between growth temperature and peak width was found, indicating that temperature does not have an effect on these properties. In general, these peaks were broader than those in CdTe films. This indicates greater strain in ZnTe, which was expected considering the lattice mismatch between ZnTe and sapphire is much greater than between CdTe and sapphire. In addition, the normal (111) peaks from the ZnTe films were narrower than the in-plane (111) peaks, indicating greater misalignment in-plane than between planes. This result is consistent with a strained ZnTe-sapphire interface.
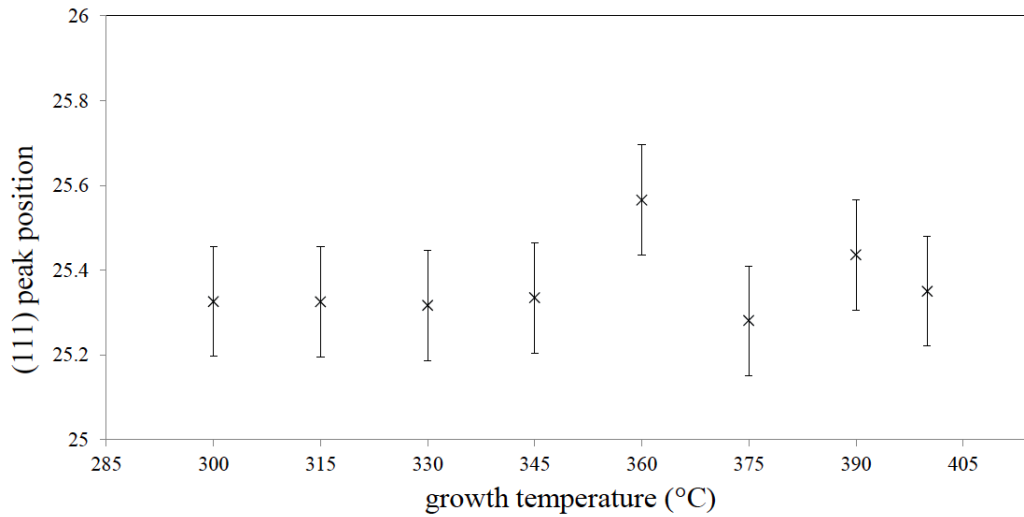
Figure 3.6: Position of the (111) peak in ZnTe films grown at various temperatures.
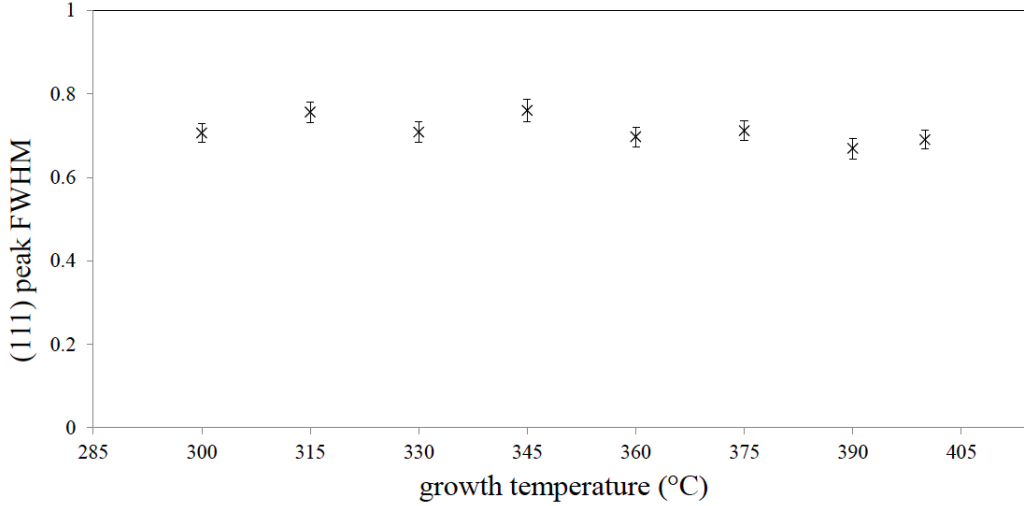
Figure 3.7: Full-width half maximum (FWHM) of in-plane (111) peaks grown at various temperatures.

The thickness of the ZnTe films was expected to decrease with increasing growth temperature, as re-evaporation becomes more probable at higher temperatures. The mean lifetime an adatom has on the surface before it is re-evaporated is given by Equation 1.2. If $k_B T$ increases, τ_A decreases, meaning that the lifetime of adsorbed atoms is shorter, and the rate of re-evaporation is higher. To verify this, the relative thickness of the films were compared. This was done by determining the intensity of the sapphire peaks and comparing this to the total intensity of the (111) film peaks and sapphire peaks in the pole figure. The procedure for doing so was similar to that used to find the B/(A+B) ratio in the CdTe film study. Here, B/(S+B) is calculated, with S representing the maximum intensity of the sapphire peaks, and B referring to the intensity of the (111) film peaks. If the value of B/(S+B) approaches 0, this means that there is very little signal from the film compared to the substrate. The film must then be thinner than a sample where the B/(S+B) value is larger. The result of this calculation is summarized in Fig. 3.8. The trend was that a higher fraction of the total intensity came from the sapphire

peaks at higher growth temperatures, indicating thinner films. Fluctuations in the trend can be attributed to inconsistencies in the growth parameters, such as chamber pressure or laser power, which are difficult to maintain constant for all growths. A sample grown at 420 ° C produced a patchy film in one corner of the substrate, but no film on the majority of the substrate.
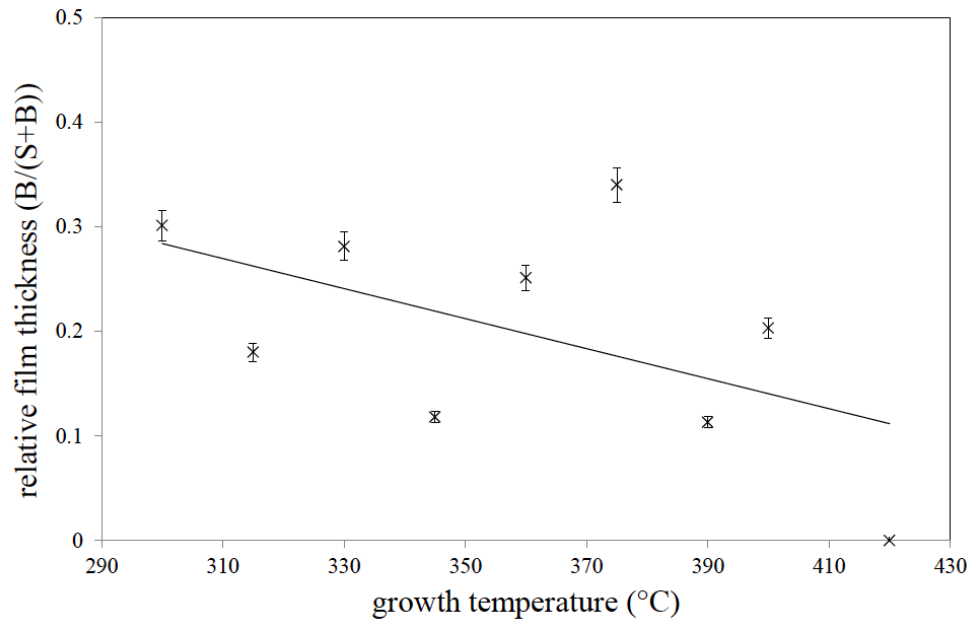
Figure 3.8: Relative thickness of ZnTe films grown at various temperatures.

The results of the study of ZnTe thin films grown at various temperatures indicate that higher quality materials are deposited at higher temperatures. The density of second-order twin defects was found to be reduced as temperature increased, while the effect of strain between the film and substrate did not appear to depend on temperature. However, the films also become thinner at higher temperatures due to desorption processes. In order to produce higher volumes of better quality materials, a compromise between quality and growth rate will need to be reached and may involve growth at an intermediate temperature (eg. 350° C).

In addition, ZnTe films were found to nucleate only B domains when grown on sapphire, regardless of the growth temperature. This differs from the growth of CdTe on sapphire, which dominantly forms A domains, but nucleate some B domains as well in almost all cases. This is due to the reduced symmetry of the sapphire surface by surface atoms, creating a three-fold symmetric surface and two types of sites a film may nucleate (i.e. A and B domains). The differing cations in CdTe and ZnTe appear to result in different preferences as to which domain forms. This result offers a possible method of controlling domain formation in ZnTe, CdTe, and potentially $Cd_xZn_{1-x}Te$ compounds.

3.1.2 Optical Comparison

A comparison of the optical properties of CdTe and ZnTe was also of interest. For bulk ZnTe materials, the band gap is direct and reported to be 2.20 ± 0.10 eV at room temperature [61]. For CdTe, the band gap is 1.45 ± 0.10 eV [5][12]. The expected Tauc plot for each of these materials was first plotted using numerical data sets of the absorption coefficient at various wavelengths [62]. The band gaps obtained by the Tauc method (2.25 ± 0.23 eV for ZnTe and 1.51 ± 0.32 eV for CdTe) were in agreement with values reported in the literature (Fig. 3.9 and Fig. 3.10 respectively).
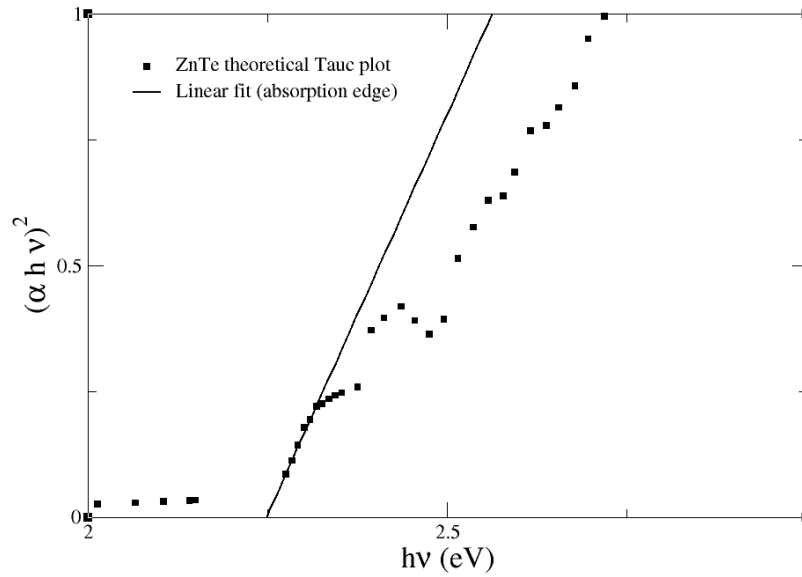
Figure 3.9: Tauc plot for ZnTe generated using data on optical constants. The band gap was determined to be 2.25 ± 0.23 eV using the Tauc method.
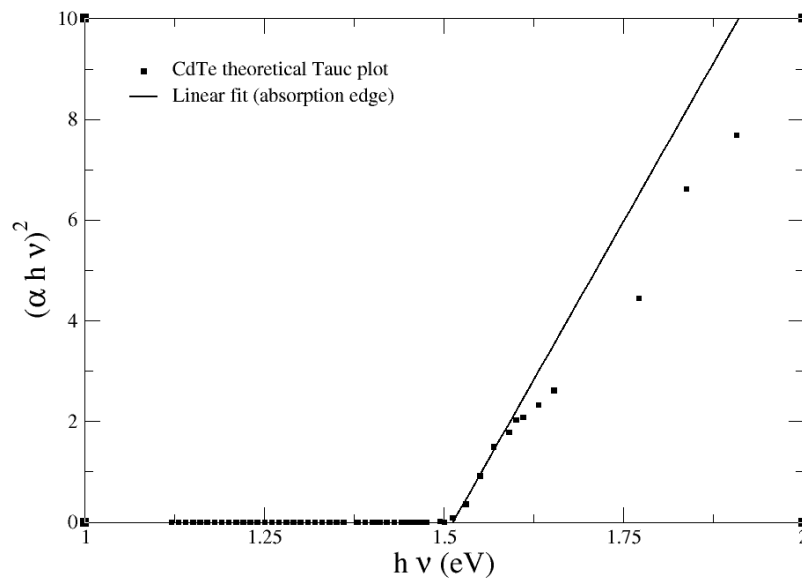
Figure 3.10: Tauc plot for CdTe generated using data on optical constants. Using this method, the band gap was determined to be 1.51 ± 0.32 eV.

Growth temperature ($^\circ$ C)	E_g (eV)
300	2.21 ± 0.06
315	2.17 ± 0.04
330	2.08 ± 0.03
345	2.19 ± 0.06

Table 3.1: Band gap energies of ZnTe films grown at various temperatures, determined using the Tauc method.
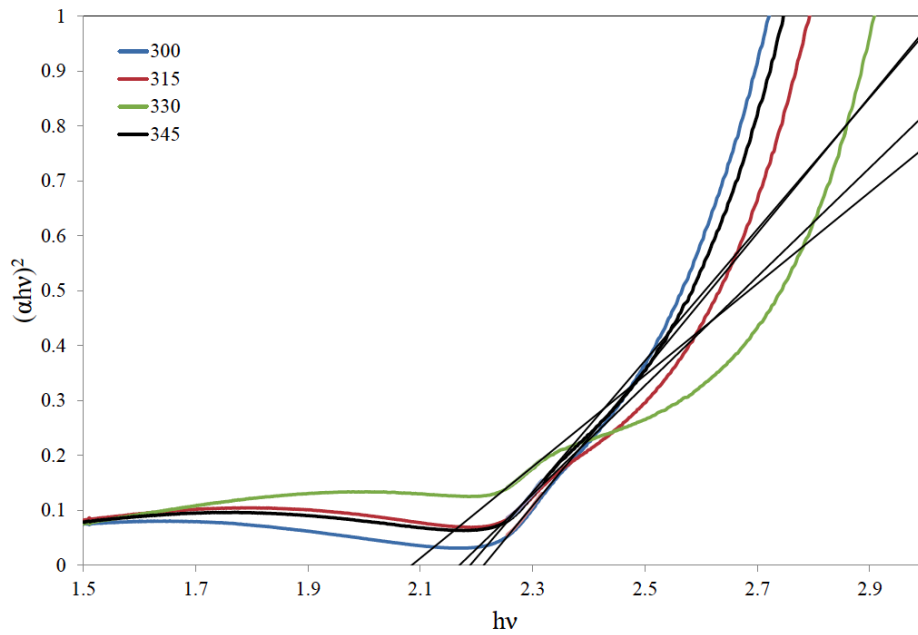
Figure 3.11: Tauc plots of ZnTe films grown at various temperatures with the linear region extrapolated to obtain the band gap energy.

The optical absorption of ZnTe films grown at temperatures between $300 -$ $345°$ C were measured using a Varian Cary 50 Spectrometer. The absorption spectrum of a bare sapphire substrate was subtracted from the ZnTe spectra prior to analysis. The Tauc plots are superimposed in Fig. 3.11, and the linear region is extrapolated to zero absorption to extract the band gap energy. All the calculated band gap energies were consistent with the expected value, and are summarized in Table 1.

A comparison of the optical absorption of CdTe and ZnTe films is also shown in Fig. 3.12. The measured band gap for the CdTe film deposited at $300°$ for 120 minutes was 1.40 ± 0.05 eV. These results suggest that the growth temperature does not strongly affect the electronic structure of the material. Since the defect density in these samples was low, and the thickness did not vary substantially, this result was not unexpected.
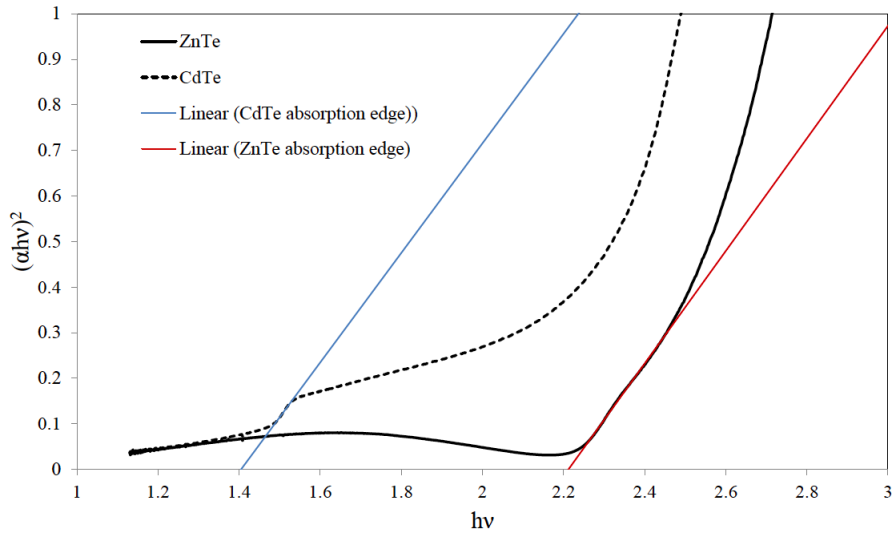
Figure 3.12: Comparison of the optical absorption from CdTe and ZnTe films grown on sapphire. The band gap energies determined by the Tauc method are indicated.

3.1.3   Growth Rates

Atomic force microscopy (AFM) was used to quantify the thickness of ZnTe deposited on sapphire per growth time. First, a Veeco diCaliber AFM was used to characterize surface roughness and film thickness from topological height scans in tapping mode. The surface roughness of a 2 minute deposition was compared to a bare sapphire substrate (it will later be shown that a 2 minute deposition time is sufficient to form a complete ZnTe layer on sapphire). For both samples, small, tall features were scattered over the surface, which was otherwise very smooth (Fig. 3.13). These features could be from sapphire dust that is created during the wafer dicing process and deposited on the surface. Although the sapphire is cleaned before growth, this type of particle would be difficult to remove. Besides these features, which are easily identifiable, fluctuations in the height of the film were small enough (less than 1 nm) that the thickness of thin films could reliably be measured by this technique.

A 12 minute ZnTe deposition was used to measure film thickness by scratching the surface of the film with the back of a scalpel. Finding the scratch using an AFM can be difficult, especially when the film and substrate are transparent, but can be identified by a change in topographical height, accompanied by mounds on either side of the scratch were material is pushed away by the scalpel. Three areas along the scratch were measured, with the change in height being equal to 7 ± 1 nm. Sapphire is a very hard material and it is unlikely that a scalpel would be able to scratch the surface, so this height is assumed to be the thickness of the deposited film. Assuming the growth rate is constant after the first complete layer of material is deposited, the thickness of films grown with various deposition times can be approximated. This works out to about 5.8 ± 0.8 nm per minute, or 0.19 ± 0.03Å per laser pulse (at 0.5 Hz repetition rate).
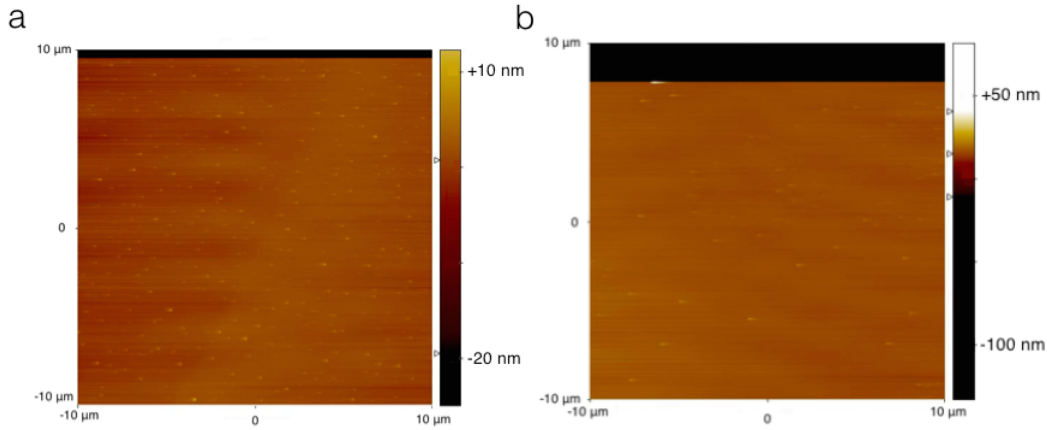
Figure 3.13: AFM height topography images of a) bare sapphire substrate and b) 2 minute growth of ZnTe on sapphire. Images taken by Matilda Backholm.

3.1.4   Film - Substrate Interface

An investigation of the sapphire-ZnTe interface began with high-resolution scanning transmission electron microscopy (STEM) to image the atomic structure in this region. A sample was prepared in the Canadian Centre for Electron Microscopy (CCEM) at McMaster University by technical staff, using focused ion beam (FIB) etching and nano-milling to thin the sample to electron transparency. TEM images of the sample were taken by an experienced user on the FEI Titan 80-300 HB microscope, also at the CCEM. As can be seen in Fig. 3.14, regular atomic ordering is observed within the film, but the structure is unclear within the first 2-3 monolayers at the interface. Electron energy-loss spectroscopy (EELS) was used to create a map of the elemental composition across the interface to possibly reveal information not evident from TEM images. Results from this analysis are shown in Fig. 3.15 and depict a transition from substrate elements to film elements as expected. The gradual transition from film to substrate (as opposed to a sharp cut-off) is likely due to a combination of instrumental limitations and material imperfections. Any measurements taken by the instrument will have a resolution width where an area of the material is

sampled. If this width encompasses regions from the film and substrate, a signal from both will be recorded. In addition, if the interface is not ideal, meaning that the substrate is not perfectly flat and contains steps, it becomes more likely that a region exists where both the film and substrate contribute to the signal. Since this gradual transition takes place over about a 1 nm length scale, which is within the resolution of this technique, a stepped interface is probable as opposed to an intermixed region.
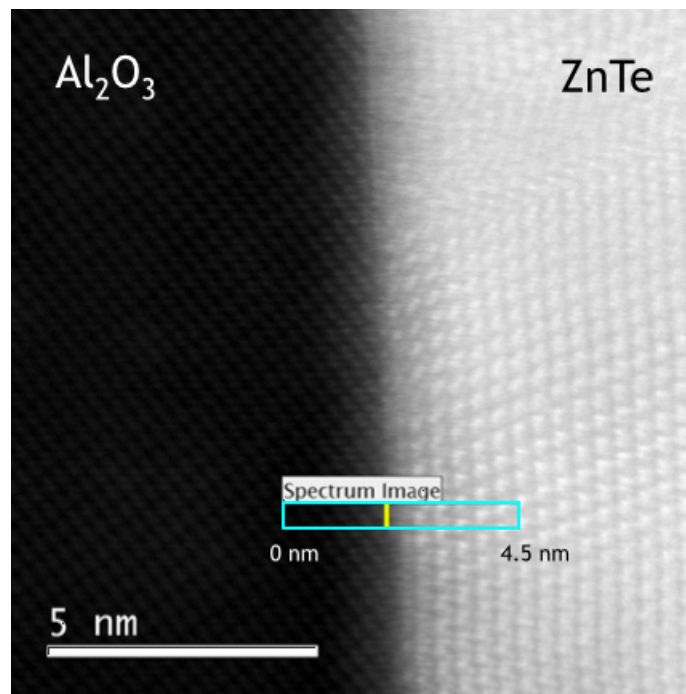
Figure 3.14: TEM image of the ZnTe-sapphire interface with the area used for EELS highlighted. Image taken by Dr. Guozhen Zhu.

A possible reason for the blurred TEM images near the interface is that there are dislocations in the sample. The presence of dislocations is probable, given the lattice mismatch between ZnTe and sapphire is 9.9%. Initially, the lattice of the film is stretched to accommodate the lattice of the substrate, and as it grows it may become energetically favourable to create a dislocation to relieve
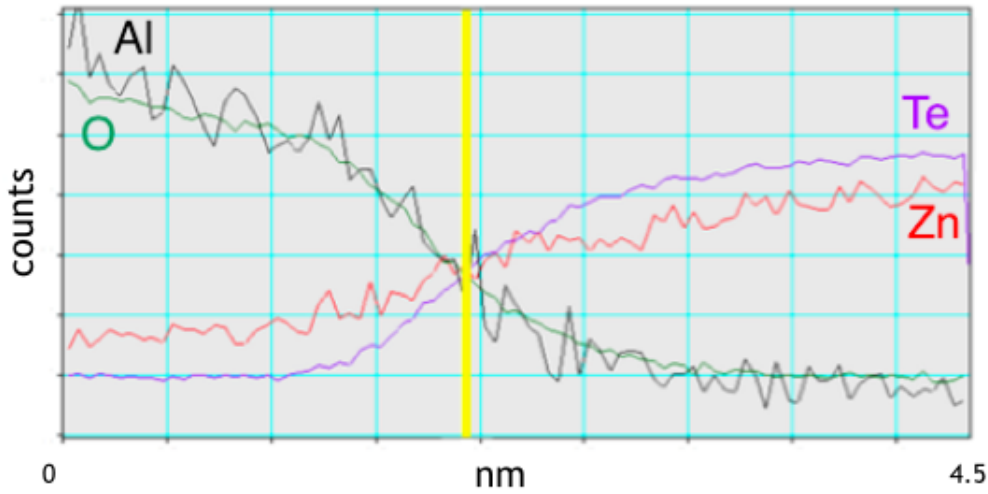
Figure 3.15: Elemental composition across ZnTe-sapphire interface from EELS. Data processed by Dr. Guozhen Zhu.

some of the stress. Fast Fourier transformation (FFT) filtering was done on select TEM images to better identify the presence of dislocations. Applying FFT to a TEM image produces a diffractogram with each peak corresponding to a set of periodic planes in the image. A particular set of peaks is selected by applying a mask to the diffractogram, and by inverse Fourier transformation, this produces an image of the selected set of planes. Discontinuities in the planes, and the addition or loss of planes, can indicate misfit dislocations [63]. Because one set of Bragg peaks does not represent the same set of planes in the film as in the substrate, drawing conclusions about the area near the interface was difficult. Additional images taken with the Phillips CM12 TEM microscope were obtained to compare with FFT filtering results. Fringes with modulating intensity were observed in the [112] film direction along the interface (Fig. 3.16). Fringes at the interface can be expected in systems where the film and substrate have different crystal structures, since there will be interference between the different sets of planes. However, the modulation of the fringes suggests that dislocations are present, as local changes in the lattice spacings could produce the observed result [15]. Dislocations in the [112] direction are consistent with

published results for (111) II-VI semiconductor films, which report that this is one of the planes along which dislocations prefer to form [60].
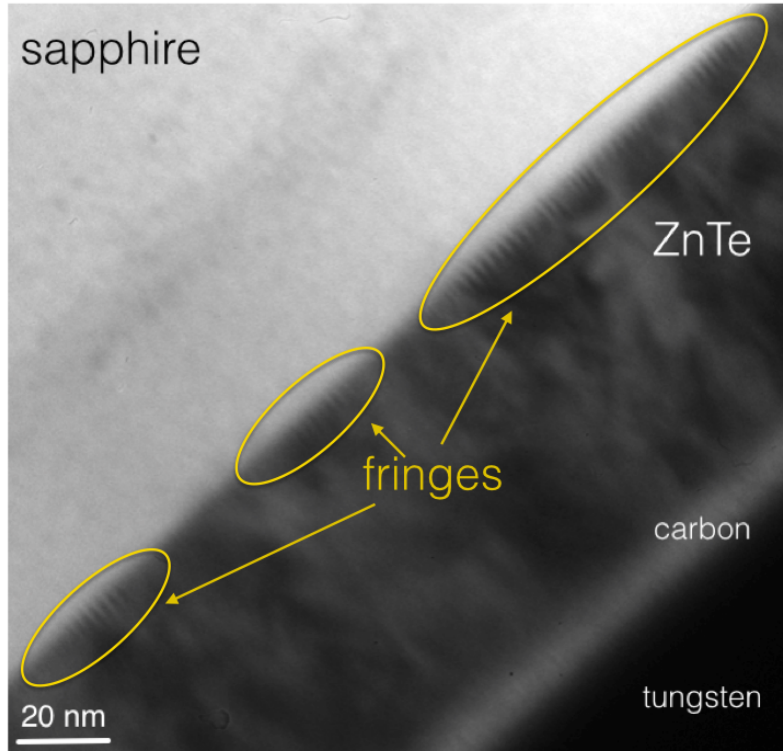
Figure 3.16: TEM image of ZnTe-sapphire interface showing fringes along the interface. Carbon and tungsten layers remain from FIB sample preparation. Image taken by Steffi Woo.

Auger electron spectroscopy was used to create an elemental depth profile through a CdTe film to compare with ZnTe-sapphire results from TEM and EELS. Instrument operation and data analysis were completed by a CCEM technician. An Ar ion beam was used to etch the sample for 10 second intervals. The etching rate was unknown since the film thickness had not been precisely measured and CdTe is not a standard material. An energy range associated with characteristic Cd, Te, O, and Al peaks was chosen to decrease run time, and the measured peaks were fit to standards for Cd, Te, and Al_2O_3. The elemental

composition measured after each etch interval was normalized so that the total composition summed to 1. The resulting depth profile is shown in Fig. 3.17. The difference in Cd and Te atomic percentage can be attributed to a difference in etching rates between these two materials and the possible intermixing of these elements throughout the ion etching process. To make the film-substrate interface more apparent, the sum of Cd and Te atomic percentages(from the film) is plotted with the sum of Al and O (from the substrate) in the inset of Fig. 3.17. The behaviour near the interface is very similar to that obtained from EELS for a ZnTe sample, with no abnormalities in composition.
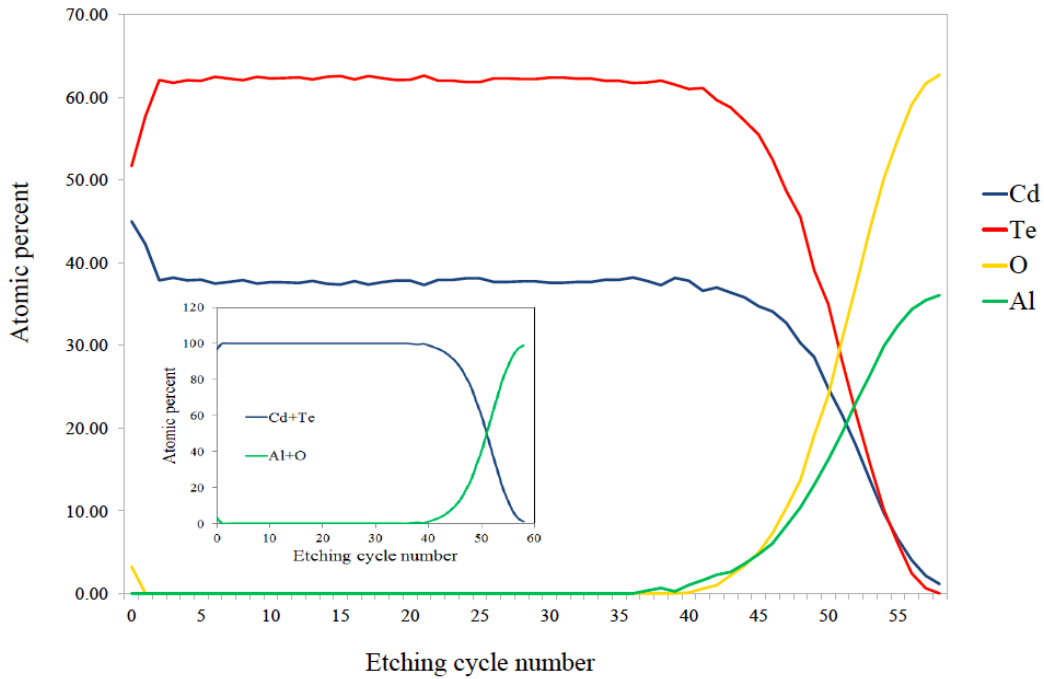
Figure 3.17: AES depth profile of the elemental composition in a CdTe film grown on sapphire. Inset: the total atomic percentage of the film and substrate elements to better visualize the interface.

3.1.5   Applications: Lift-off

The transfer of a ZnTe film from sapphire to polysulfone was attempted to verify if the lift-off technique could be applied to films other than CdTe. The quality of the transferred film was characterized using XRD texture analysis and scanning electron microscopy (SEM).

The pole figure of the ZnTe film before and after lift-off are compared in Fig. 3.18. The same peaks appear with similar intensity and width (except for the disappearance of the sapphire peaks), confirming that the lift-off process does not alter the structure of the film. Fig. 3.19 shows SEM images of the film transferred to polysulfone and the remaining sapphire substrate taken with

the JEOL JSM-7000F in the CCEM. The surface of the transferred film was uniform over large length scales (on the order of micrometers), and where there was cracking around the outside of the film, the edges are sharp with little buckling or peeling. These results suggest that the quality of the film remains intact throughout the lift-off process, and that the film can be removed in a single piece without inducing significant defects.

The physics of why the film is able to lift-off is not well understood, and may even be contrary to initial expectations. In order to drive epitaxial alignment, the interaction between the film and substrate is expected to be strong, yet the films are removed with little force. As well, the entire film can lift-off in one piece, which is surprising given the relative surface area to thickness: 12 mm by 12 mm square, but only on the order of 100 nm thick. Analysis of the film-substrate characterization suggests that dislocations may lie at the interface, which would reduce the interaction strength between the film and substrate atoms. However, a better understanding of this phenomenon is required in order to improve the lift-off process and identify limitations for its use.
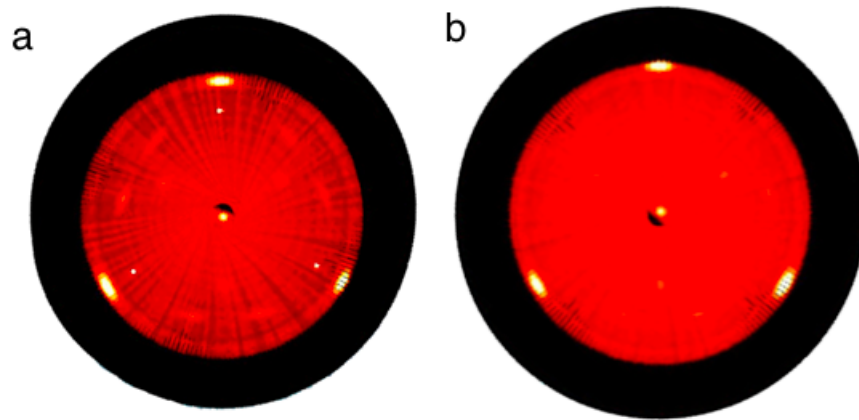
Figure 3.18: (111) pole figures of a) ZnTe on sapphire and b) ZnTe transferred to polysulfone.
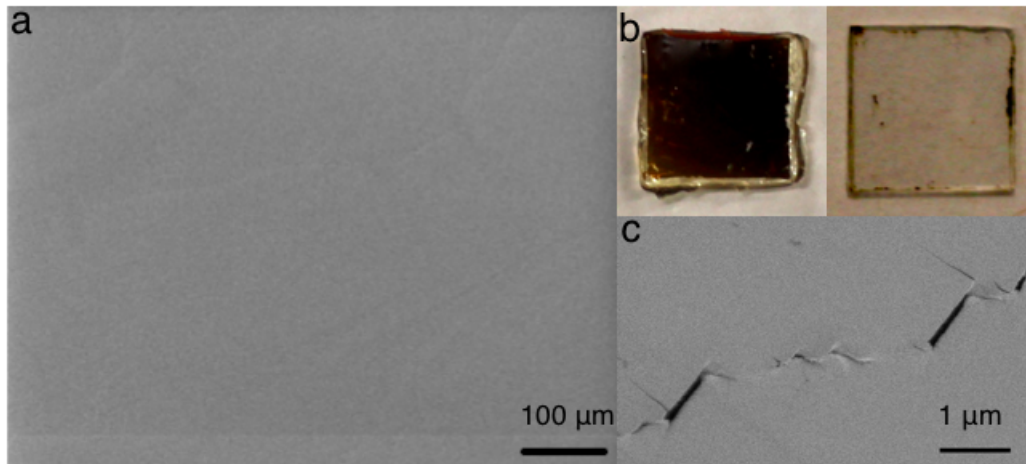
Figure 3.19: a) SEM image of a ZnTe film transferred to polysufone, near the centre of the film b) CdTe on polysulfone (left) and sapphire substrate (right) after lift-off c) SEM image of ZnTe on polysulfone, near an edge.

3.2   Growth of CdTe/ZnTe Bilayer Films

The growth of CdTe on ZnTe and vice versa is very different from the growth of these materials on sapphire: Both ZnTe and CdTe share the same cubic, zinc blende crystal structure, with a lattice mismatch of 6.2%. This allows for more options in the epitaxial growth of one material on the other, compared to the growth of each material on sapphire, since more lattice matched surfaces are available. The 6.2% mismatch falls between the CdTe-sapphire mismatch (4.2%) and the ZnTe-sapphire mismatch (9.9%), creating an intermediate degree of strain in the system. Also, both CdTe and ZnTe are more easily deformed than sapphire, allowing for increased flexibility in the manipulation of the material's resulting properties. To begin studying the growth of multilayer CdTe/ZnTe films, bilayers composed of one material on the other were first grown. To accomplish this, ZnTe was deposited on sapphire at 300° C for 60 minutes, with a laser energy of 80 mJ and 0.5 Hz repetition rate. Immediately after this first deposition was complete, the target was manually changed to CdTe without breaking vacuum by rotating a shaft coupled to the target mount inside the growth chamber. A layer of CdTe was then deposited on the existing film for another 60 minutes with the same laser parameters. The reverse (ZnTe grown on CdTe) was also fabricated the same way.

3.2.1   Structural Analysis

A uniform crystal structure is important in establishing consistent material properties. Defects that arise during the growth process can significantly impact the structure of the film, causing complications if commercial applications are desired. This is of particular concern in multilayer structures since the lattice mismatch at the interface between successive layers can induce strain related dislocations.

To begin an investigation into the structure of CdTe/ZnTe bilayer films, XRD data was collected for the two bilayer samples described above. Since (111) CdTe and ZnTe prefer to take on different orientations when grown on sapphire, a comparison of the resulting crystal structure was of interest. Scans were collected at 0.5° slicing for 10 seconds per frame to better resolve the two sets of peaks. The peaks from each material could be separated in order to create individual pole figures for CdTe and ZnTe by setting the 2θ integration range around each peak to cover values only up to the point they begin to overlap. This way, the intensity at each 2θ only contributes to either the CdTe peak or the ZnTe peak (Fig. 3.20).
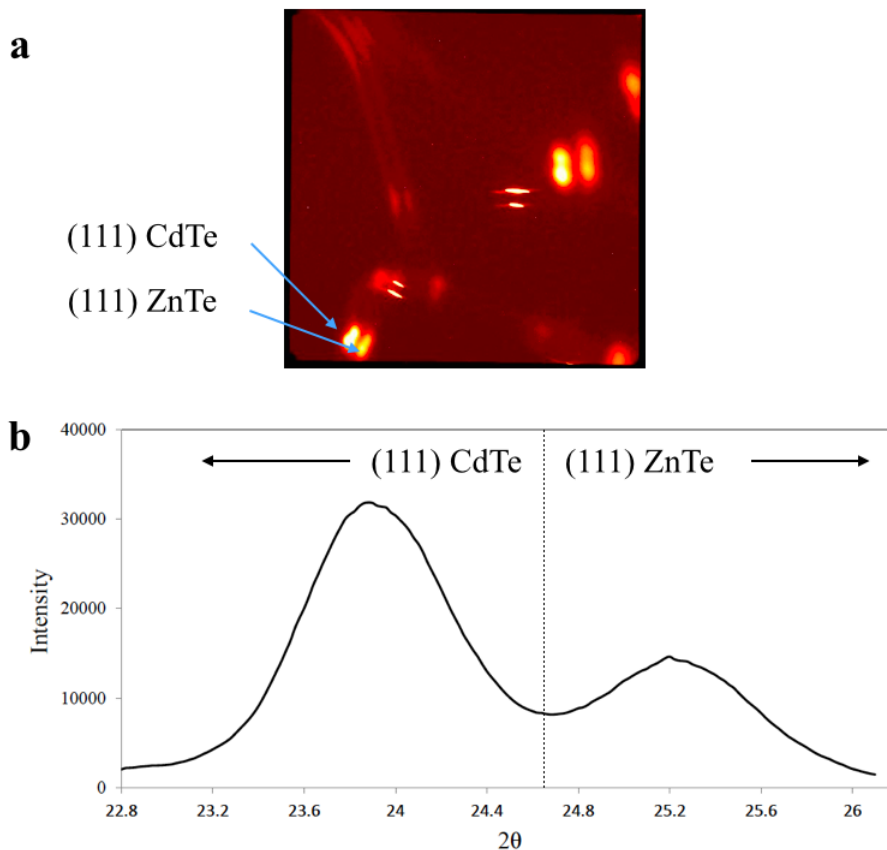
Figure 3.20: a) ϕ 360 scan of a CdTe/ZnTe bilayer films. b) The intensity of the (111) peaks from CdTe and ZnTe layers integrated along 2θ. Values to the left of the dotted line were used to produce the CdTe (111) pole figure, and values to the right were used to produce the ZnTe (111) pole figure.

Fig. 3.21 shows the (111) pole figures for both the CdTe and ZnTe layers in the two samples. In both cases, the first layer deposited on sapphire took its usual orientation: only one domain for ZnTe, and multiple domain formation for CdTe. However, the more interesting feature is that in both structures, the first and second layers have the *same* crystal structure. That is, if ZnTe is deposited first, the CdTe layer grown on top will grow in the same orientation. A comparison of the first and second-order twin densities yielded almost identical values in both layers of the same sample, indicating that even structural defects are preserved between layers. This suggests that a uniform structure in multilayer films, which would be comprised of multiple sets of these bilayers, is possible.
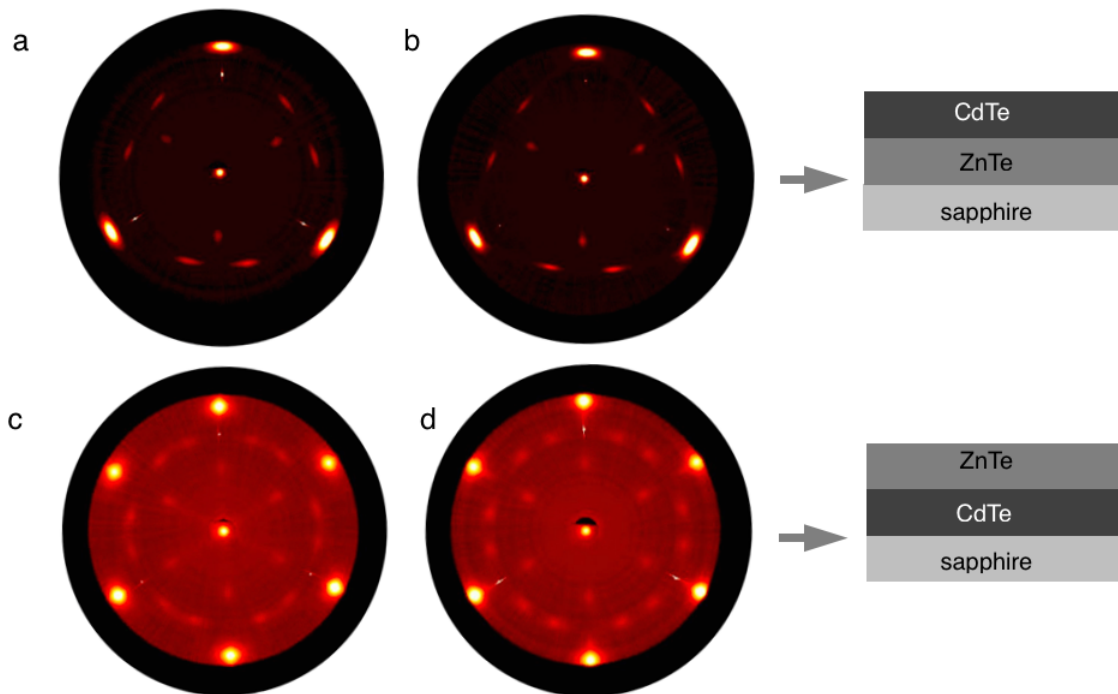
Figure 3.21: (111) pole figures for bilayers: a) ZnTe on sapphire b) CdTe on ZnTe c) CdTe on sapphire d) ZnTe on CdTe.

3.2.2   Layer Intermixing

When constructing films composed of multiple layers, there is a possibility that the layers do not form separately, but instead intermix as a result of diffusion across the interface. This can have a dramatic effect on the properties of a material, since morphology is strongly tied to the band structure, and thus the electrical and optical properties [64]. Because of this, an understanding of the factors contributing to layer intermixing, and how it can be controlled, is an important component in the study of multilayer films.

From the X-ray diffraction data collected for both samples, the peaks associated with ZnTe and CdTe layers are well resolved and easily distinguishable, indicating that there is little intermixing or diffusion between the two layers. If the layers were intermixed, the peaks from each material would not be resolvable, and instead a broad signal encompassing the same 2θ range would be observed. The XRD powder pattern obtained from MAX3D software for one of the bilayers is shown below in Fig. 3.22. The position of the (111) CdTe and ZnTe peaks were determined to be 23.90° and 25.22° respectively. The CdTe peak is shifted to higher 2θ, and ZnTe is shifted to lower 2θ, relative to their positions in single-layer films. This is expected because the CdTe unit cell is compressed while the ZnTe unit cell is stretched, due to lattice mismatch, and suggests that both layers are strained as opposed to strain-relaxed as in the single-layer case.
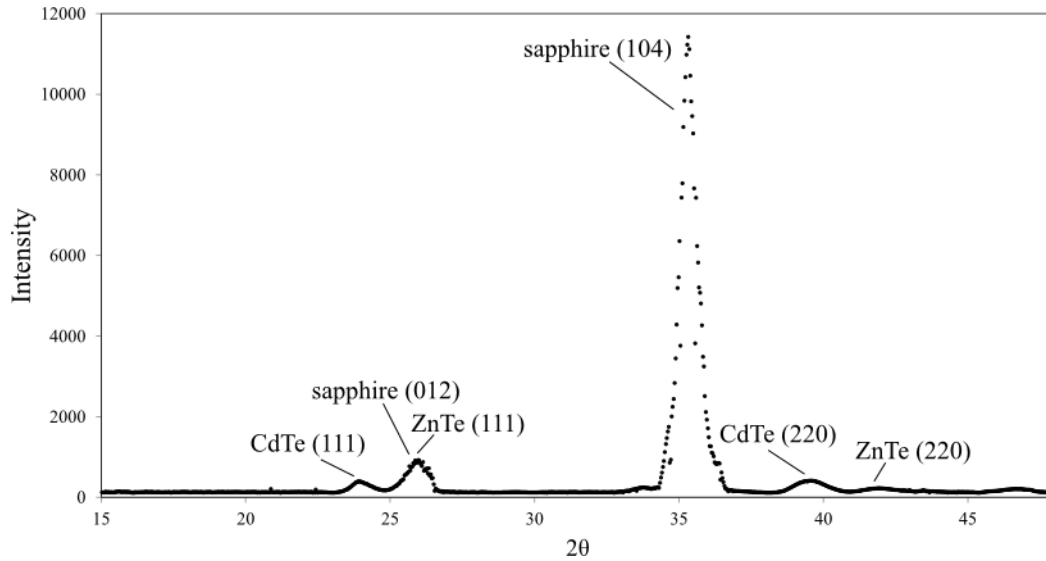
Figure 3.22: Powder pattern of a CdTe/ZnTe bilayer film grown on sapphire, generated by MAX3D software.
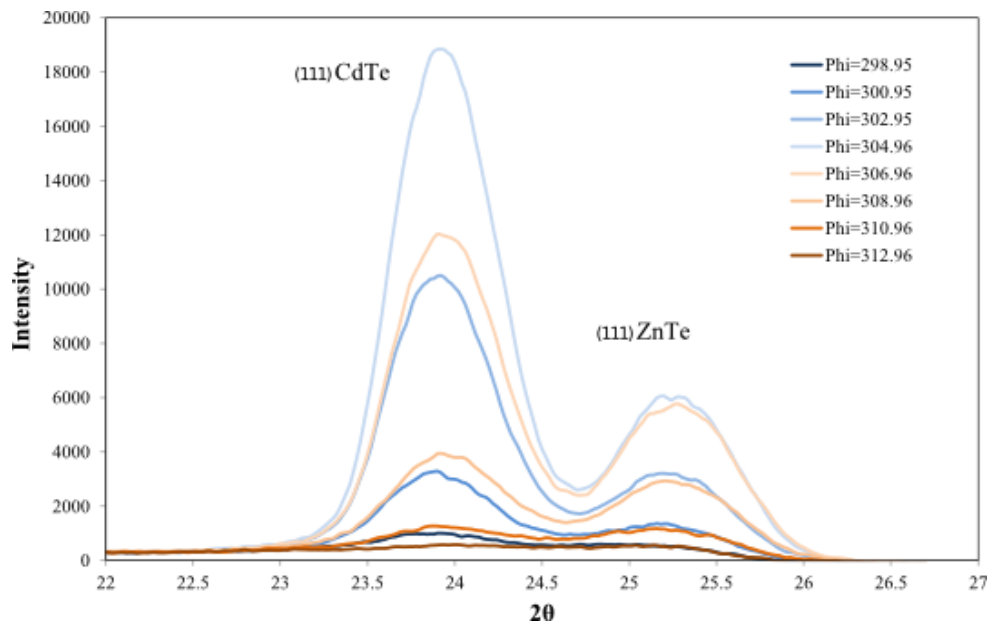
Figure 3.23: (111) peaks of CdTe and ZnTe collected by XRD for a bilayer sample as the ϕ position is rotated through the diffraction condition.

To further illustrate the absence of intermixing, the (111) peaks of CdTe and ZnTe were observed to remain distinct when stepping through individual

XRD frames obtained from a ϕ scan. As the peaks come in and out of their diffraction condition, the intensity in both increases and decreases, without any intermediate peak formation (Fig. 3.23).

3.2.3   Control of Domain Formation in CdTe

The result that ZnTe reliably forms only one domain when grown on sapphire has additional implications: This provides a means of also obtaining single domain CdTe by depositing a thin seed layer of ZnTe first. Based on results previously described, the CdTe layer on top would maintain the same structure as the ZnTe layer, and yield improved crystal quality as long as there was enough ZnTe deposited to completely cover the sapphire surface first. The minimum thickness necessary for the seed layer deposition was an interesting question, as this would also reveal information on the growth mechanism of ZnTe on sapphire.

To investigate this further, ZnTe seed layers of various thickness were deposited on sapphire, with a thicker layer of CdTe deposited on top. The structure of the films were characterized by XRD texture analysis. If the CdTe layer maintained the same orientation as the ZnTe layer, which reliably takes on the same orientation when deposited on sapphire, this would indicate that a complete layer of ZnTe was formed first. If the CdTe was found to form multiple domains, this would suggest the ZnTe formed in islands, with areas of exposed sapphire where CdTe growth could nucleate.

The resulting CdTe (111) pole figures are shown in Fig. 3.24 for ZnTe layers of 2, 1.75, 1.5, 1.25, and 1 minute deposition times. CdTe was found to maintain a single domain, consistent with ZnTe, down to 1.25 minutes of seed layer deposition. This suggests that for deposition times less than 1 minute, the sapphire surface only has partial coverage. From AFM film thickness measurements, a complete layer, requiring 1.25 minutes of deposition,

would roughly correspond to 0.73 ± 0.10 nm of material. This corresponds to 2-3 atomic layers, with the thickness of one atomic layer being roughly 0.26 nm. Since this represents the first measurement where a complete layer was formed, and not necessarily the minimum amount of material required to form a complete layer, layer-by-layer growth seems the most likely mode for this system. The 9.9% lattice mismatch between the film and substrate creates strain at the interface, and it is possible that the growth mode changes to layer-plus-island as the film continues to grow beyond the critical thickness and dislocations are introduced. This is supported by XRD evidence that the films are strain-relaxed, which would not be possible without the introduction of defects.
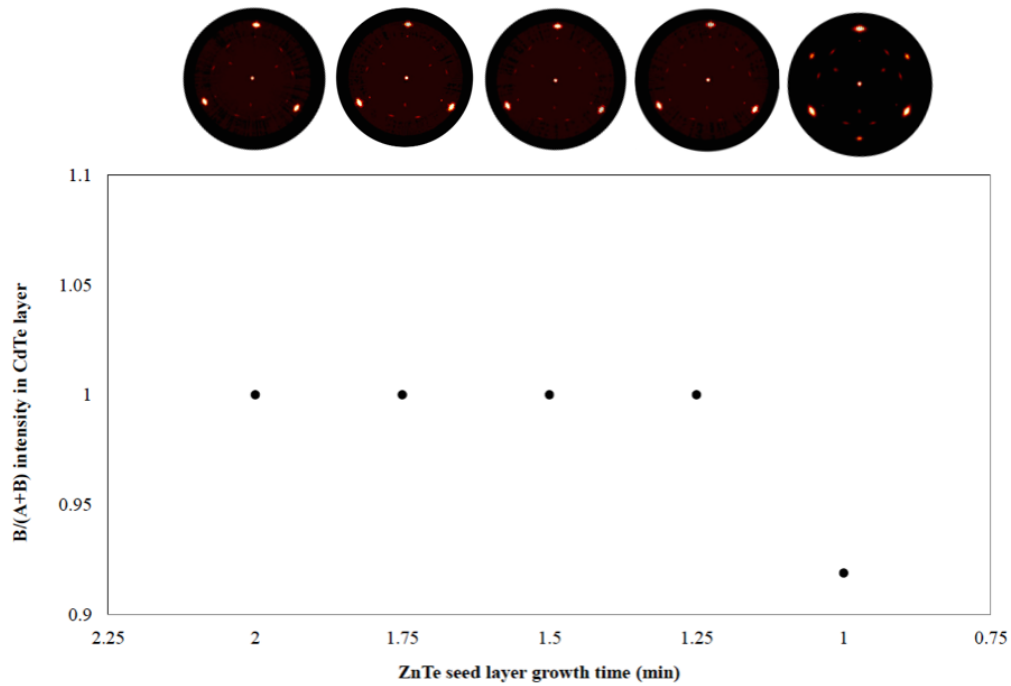
Figure 3.24: CdTe (111) pole figures grown on ZnTe layers with various deposition times and the corresponding B/(A+B) intensity ratio.

3.3   Growth and Characterization of CdTe/ZnTe Multilayer Films

An investigation into the growth of CdTe/ZnTe multilayer films was initiated to study the impact of additional layers on the previously characterized bilayer case. Samples were grown under the same conditions as the bilayer samples for a total time of 120 minutes, with the deposition time of each layer varying. Each sample began with a ZnTe deposition to seed a predictable orientation, followed by a CdTe deposition, and ending with an additional ZnTe layer. The CdTe deposition time was varied, with the two outside ZnTe layers taking on equal deposition times that give the film a total growth time of 120 minutes. For example, if the CdTe layer was deposited for 20 minutes, each ZnTe layer would be deposited for 50 minutes.

3.3.1   Structural Analysis

XRD characterization was conducted for samples grown at 300° C with 2 and 40 minute CdTe deposition times. In the sample with the thin CdTe layer (2 minutes), XRD did not show any signal from CdTe, and the ZnTe signal showed multiple domains (Fig. 3.25). Since ZnTe deposited on sapphire does not nucleate multiple domains, the defects must result from the addition of the third layer. This result was unexpected because bilayers of ZnTe on CdTe, although twinned, had the same orientation. This was also the case for CdTe on ZnTe. The reason for this loss of symmetry is likely due to the introduction of the second CdTe-ZnTe interface, creating strain on the CdTe layer from surfaces above and below.

The sample with the thicker CdTe layer (40 minutes) allowed a signal from CdTe to be obtained from XRD. A breakdown of the symmetry was again observed in the ZnTe layers, although the degree to which this occurred was reduced. The symmetry between the first ZnTe layer and CdTe layer remained
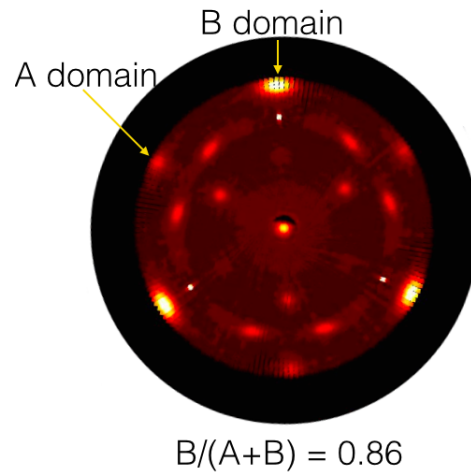
Figure 3.25: (111) pole figure for ZnTe from a sample with a 2 minute CdTe deposited layer. Both A and B domains are present and the B/(A+B) intensity ratio is indicated.

intact (Fig. 3.26). This suggests that the defect density is lower in thicker CdTe layers than in thinner layers, allowing the top ZnTe layer to grow on a comparatively relaxed CdTe surface.

The CdTe and ZnTe peaks were not as well resolved as in the bilayer case, implying that some intermixing of the layers had occurred. The film peaks were also shifted from their relaxed positions, with the CdTe peak shifting to higher 2θ and ZnTe shifting to lower 2θ. The shift in the multilayer films was greater than in the bilayer case, indicating that the amount of strain has increased. A comparison of the ZnTe and CdTe peak positions in single-layer, bilayer, and multilayer films is provided in Table 2.

The growths were repeated at 350° C to determine if an increased temperature would promote a decrease in defect density, as observed in ZnTe single-layer films. The result was an increased intermixing of the CdTe and ZnTe layers, as evidenced by a broad diffraction signal, centred around the (111) ZnTe peak
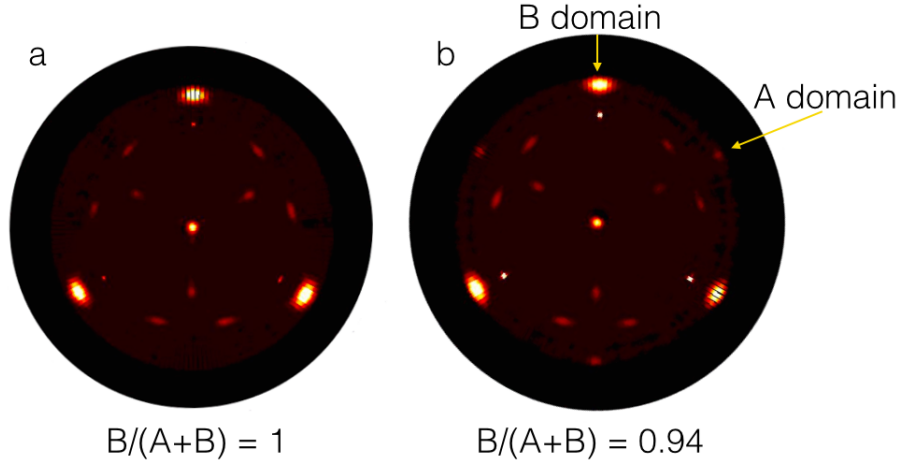
Figure 3.26: (111) pole figures of a) CdTe and b) ZnTe from a sample with a 40 minute CdTe deposited layer. The B/(A+B) intensity ratio for each layer is indicated.

Material	Peak Position (2θ)		
	Single-layer	Bilayer	Multilayer
ZnTe	25.33	25.22	25.18
CdTe	23.70	23.90	24.28

Table 3.2: CdTe and ZnTe (111) peak position in single-layer, bilayer, and multilayer films.

position. Additional films grown at intermediate temperatures show a trend indicating an increase in intermixing as the growth temperature is increased. The CdTe signal was also found to decrease as temperature increased, suggesting that less CdTe is retained in films grown at higher temperatures. These results are summarized in Fig. 3.27, which also shows the XRD data for a single-layer ZnTe and CdTe film for comparison. Temperature seems to have a greater impact on the CdTe layer, since the shift in this peak is greater than the shift in the ZnTe peak as temperature is increased.

Based on XRD results for single-layer ZnTe thin films, it can be assumed that the first layer of the multilayer structure is deposited with only B domains. From the study of bilayer films, we also know that the second layer takes on the same orientation as the first deposited layer, and so this should only have B domains as well. However, the addition of a third layer seems to upset this symmetry, resulting in the formation of multiple domain signals from the third layer for thicker CdTe layers, and from both materials for thinner CdTe layers. To combat this, multilayer films may need to be grown at lower temperatures to reduce the amount of diffusion and intermixing. Thicker layers also appear to improve the quality of the multilayer films. This makes sense since a smaller fraction of the material is deposited near an interface, where defects are more likely to occur due to strain effects. The successful growth of high quality bilayer films suggests that well-behaved multilayer growth is possible, though the impact of additional interfaces on the overall structure requires more investigation.
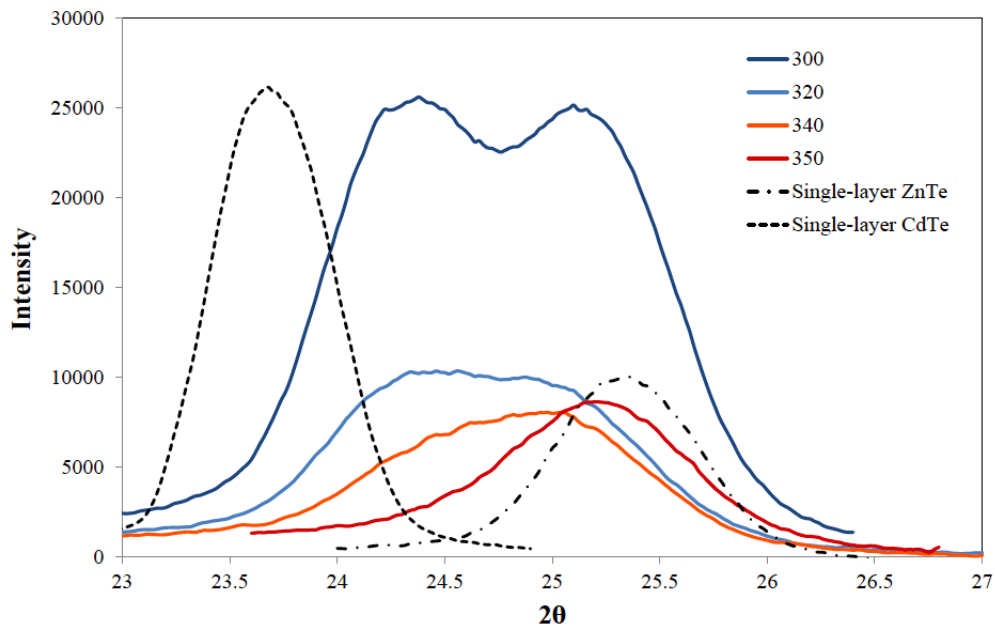
Figure 3.27: Interlayer mixing between CdTe and ZnTe layers as the growth temperature (° C) increased. (111) peak profiles for single-layer ZnTe and CdTe films are shown for comparison.

Chapter 4

Conclusions

4.1 Summary

In this work, CdTe/ ZnTe thin films and heterostructures were grown on sapphire substrates using pulsed laser deposition. The structure and optical properties of single-layer, bilayer, and multilayer films were characterized by X-ray diffraction, UV-Vis spectroscopy, atomic force microscopy, and electron imaging and spectroscopy techniques. This study was motivated by a desire to better understand the growth mechanisms involved in the formation of these structures, and how growth parameters such as temperature, deposition time, and relative layer thickness, affect their overall properties.

The growth of (111) ZnTe on (0001) sapphire was found to differ from the growth of (111) CdTe, despite their structural similarities. While two distinct domains are found to form in CdTe growth, only one of these domains formed in ZnTe. This phenomenon appears to be independent of the growth temperature and deposition time. The origin of multiple domain formation, although a common defect in II-VI semiconductors, is not currently well understood. However, it is thought that these domains nucleate at the beginning of growth, indicating that the differing cations interact with the surface of the substrate in unique ways. Second-order twin defects were observed in ZnTe films at all

tested growth temperatures (300-400° C), with a decrease in defect density at higher temperatures, likely resulting from an increased surface diffusion energy. Film thickness was also found to decrease at higher temperatures, due to re-evaporative processes, with no film being deposited at 420° C. No correlation between growth temperature and peak position or FWHM was found, suggesting that strain is not reduced in higher temperature growths, and that the films are overall strain-relaxed. TEM analysis of the ZnTe-sapphire interface suggests that misfit dislocations form in the interface plane, which may contribute to the release mechanism these films demonstrate. EELS and AES characterization of the ZnTe-sapphire and CdTe-sapphire interfaces respectively showed similar results and indicate a gradual transition from film to substrate over about a 1 nm length scale, possibly due to a non-ideal interface and instrument resolution.

The band gap of ZnTe and CdTe films were determined using the Tauc method and found to be in agreement with values reported in the literature (2.21 ± 0.1 eV for ZnTe and 1.45 ± 0.1 eV for CdTe). The band gap of ZnTe films grown at different temperatures were found to have roughly the same band gap, ranging from 2.08 ± 0.03 eV to 2.21 ± 0.06 eV. This suggests that growth temperature does not have an effect on the electronic structure of ZnTe thin films. Since it was found that the films are overall strain-relaxed, with a low defect density, the electronic structure was not expected to differ significantly from bulk properties.

Bilayer films, composed of CdTe grown on ZnTe and vice versa, were found to maintain a constant structure throughout both layers. That is, the material grown on the top layer had an orientation defined by the bottom layer, regardless of whether CdTe or ZnTe was deposited first. This led to an investigation aimed at controlling domain formation in CdTe, which has a tendency to form multiple domains when deposited on sapphire, and has previously been difficult to overcome consistently. Single-domain ZnTe is consistently deposited on sapphire, allowing for control of this issue. The minimum amount of ZnTe

needed for complete coverage of the substrate was determined to be 0.73 ± 0.1 nm, based on AFM film thickness measurements and XRD texture analysis (assuming a constant, linear growth rate). This suggests that the growth mode is layer-by-layer, or possibly layer-plus-island, since 0.73 ± 0.1 nm corresponds to approximately 2-3 monolayers of material. In addition, XRD results showed distinct sets of peaks from both materials in bilayer films, indicating independent layer formation without intermixing. These results demonstrate that high quality CdTe/ZnTe bilayer films are grown by pulsed laser deposition on sapphire, and that using ZnTe as a seed layer, nearly single-crystal CdTe and ZnTe films can be reproduced consistently.

The growth of multilayer films was initiated based on results previously obtained from the bilayer study. The addition of a third layer resulted in a breakdown of the maintained structure, with texture analysis showing some amount of multiple domain formation in all samples studied. This may be due to increased stress in the film caused by the additional interface. CdTe (111) peaks were found to shift to higher 2θ positions as the number of layers increased, while ZnTe (111) peaks shifted to lower 2θ, indicating increased strain in the system. Increasing the deposition time of the middle (CdTe) layer seemed to decrease the defect density, as evidenced by lower intensity peaks from secondary domains in XRD data. Temperature also appears to have an effect on the growth of these structures, with an increase in interlayer mixing as temperature was increased from 300-350° C, demonstrated by an increased overlap in CdTe and ZnTe peaks in XRD data. In order to study multilayer films with more layers, better control of layer intermixing in three layers should first be achieved.

4.2   Future Work

4.2.1   Multilayer Film Growth

The growth of multilayer films is an important field of study, motivated by the wide variety of potential applications they may have in current and new technologies. Developing methods of fabricating high quality multilayer films will aid in the advancement of these technologies, and so a better understanding of the growth mechanisms involved and how they may be controlled should be further studied.

The structural symmetries conserved between independent layers in bilayer films was shown to breakdown with an additional layer, resulting in defects and layer intermixing. A detailed investigation into the effects of various growth parameters on the overall structure may provide insight into how this issue can be overcome. In addition, characterization of the CdTe-ZnTe interface may also provide important information about how these materials grow and help identify the cause of their structural problems. The addition of more layers and the effect on material structure and properties should also be studied.

4.2.2   Automated Target Rotator for Pulsed Laser Deposition of Multilayer Films

In order to grow multilayer films, the target material needs to be alternated throughout the growth process. Since oxides readily form on surfaces when exposed to atmospheric pressures, this is best done while the sample remains under vacuum. An automated target rotator that moves targets mounted inside the growth chamber in and out of the laser path would allow multilayer films to be grown more quickly and reproducibly.

Work towards this has begun, with the installation of an encoder wheel to track the position of the rotator. To complete this project, a motor would need

to be connected to the rotatable shaft, and the encoder wheel would need to be programmed to start and stop movement of the target wheel when the position of a desired target is reached.

4.2.3   Thin Film Lift-off

The result that CdTe and ZnTe thin films have been found to consistently lift-off of sapphire substrates allows for many new potential applications for these materials. However, the physics of this phenomenon is not well understood and requires further study. A TEM analysis of a film-carrier interface, to compare with a film-substrate interface, may provide additional information about how the film is removed. In addition, confirming that the entire film has been removed from the sapphire substrate should also be accomplished.

It is currently postulated that misfit dislocations form at the interface as the film thickness exceeds the critical dimension, resulting in a weakening of the bonds between the film and substrate, originally formed to ensure epitaxial alignment. To test this, the lift-off of a film grown on a closely lattice matched substrate could be attempted. A much closer lattice match would result in less strain at the interface, and so a lower density of defects in this region. In addition, Raman spectroscopy measurements identifying the types of bonds formed within a CdTe or ZnTe film on sapphire may also reveal important information about the atomic bonding at the interface.

Bibliography

[1] Clare F. Macrae, Ian J. Bruno, James A. Chisholm, Paul R. Edgington, Patrick McCabe, Elna Pidcock, Lucia Rodriguez-Monge, Robin Taylor, Jacco van de Streek, and Peter A. Wood. *Mercury CSD 2.0 – new features for the visualization and investigation of crystal structures. Journal of Applied Crystallography*, 41(2):466–470, Apr 2008.

[2] B. Ghosh, D. Ghosh, S. Hussain, R. Bhar, and A.K. Pal. Growth of ZnTe films by pulsed laser deposition technique. *Journal of Alloys and Compounds*, 541(0):104 – 110, 2012.

[3] L. Reimer. *Scanning Electron Microscopy: Physics of Image Formation and Microanalysis*. Springer-Verlag, Heidelburg, second edition, 1998.

[4] X. Wu. High-efficiency polycrystalline CdTe thin-film solar cells. *Solar Energy*, 77(6):803 – 814, 2004.

[5] C.S. Ferekides, U. Balasubramanian, R. Mamazza, V. Viswanathan, H. Zhao, and D.L. Morel. CdTe thin film solar cells: device and technology issues. *Solar Energy*, 77(6):823 – 830, 2004.

[6] Y Eisen and A Shor. CdTe and CdZnTe materials for room-temperature X-ray and gamma ray detectors. *Journal of crystal growth*, 184:1302–1312, 1998.

[7] Y. Eisen, A. Shor, and I. Mardor. CdTe and CdZnTe gamma ray detectors for medical and industrial imaging systems. *Nuclear Instruments*

and Methods in Physics Research Section A: Accelerators, Spectrometers, Detectors and Associated Equipment, 428(1):158 – 170, 1999.

[8] P.J. Sellin, A.W. Davies, A. Lohstroh, M.E. Ozsan, and J. Parkin. Drift mobility and mobility-lifetime products in CdTe: Cl grown by the travelling heater method. *IEEE Transactions on Nuclear Science*, 52(6):3074–3078, 2005.

[9] R. Amutha, A. Subbarayan, R. Sathyamoorthy, K. Natarajan, and S. Velumani. Conduction studies on ZnTe thin films. *Journal of New Materials for Electrochemical Systems*, 10(1):27, 2007.

[10] W.I.Han, J. H. Lee, J. C. Choi, and H. S. Lee. Carrier dynamics and activation energy of CdTe/ZnTe nanostructures with different CdTe thicknesses. *Journal of Crystal Growth*, 370(0):307 – 310, 2013. 16th International Conference on Metalorganic Vapor Phase Epitaxy.

[11] D. Ferizovi, L. Peng, H. Sultana, P. Mukherjee, S. Witanachchi, M.C. Tamargo, and M. Muoz. Photoreflectance spectroscopy study of a strained-layer CdTe/ZnTe superlattice. *Journal of Applied Physics*, 110(9):093703, 2011.

[12] B. Späth, J. Fritsche, F. Suberlich, A. Klein, and W. Jaegermann. Studies of sputtered ZnTe films as interlayer for the CdTe thin film solar cell. *Thin Solid Films*, 480481(0):204 – 207, 2005.

[13] A. Shik. *Quantum Wells: Physics and Electronics of Two-Dimensional Systems*. World Scientific, Singapore, 1997.

[14] M.R.H. Khan. Interface properties of a CdTe-ZnTe heterojunction. *Journal of Physics D: Applied Physics*, 27(10):2190, 1994.

[15] L. Eckertova. *Physics of Thin Films*. Plenum Press, New York, second edition, 1986.

[16] H. Luth. *Solids Surfaces, Interfaces, and Thin Films.* Springer-Verlag, Berlin, fifth edition, 2010.

[17] M. Ohring. *Materials Science of Thin Films - Deposition and Structure.* Academic Press, San Diego, 2000.

[18] K. Pinardi, U. Jain, C.S. Jain, H.E. Maes, R. Van Overstraeten, and M. Willander. Critical thickness and strain relaxation in lattice mismatched II-VI semiconductor layers. *Journal of Applied Physics*, 83(9):4724–4733, 1998.

[19] V.G. Dubrovskii. *Nucleation and Growth of Nanostructures.* Springer, Berlin, 2014.

[20] W.K. Liu and M.B. Santos. *Thin Films: Heteroepitaxial Systems.* World Scientific Publishing, Singapore, 1999.

[21] B. Ray. *II-VI Compounds.* Pergamon Press, Oxford, 1969.

[22] N.W. Ashcroft and N.D. Mermin. *Solid State Physics.* Thomson Learning, United States of America, 1976.

[23] C.G. Van de Walle. Band lineups and deformation potentials in the model-solid theory. *Physical Review B*, 39(3):1871, 1989.

[24] A.R. Balu, V.S. Nagarethinam, A. Thayumanavan, K.R. Murali, C. Sanjeeviraja, and M. Jayachandran. Effect of thickness on the microstructural, optoelectronic and morphological properties of electron beam evaporated ZnTe films. *Journal of Alloys and Compounds*, 502(2):434–438, 2010.

[25] H. Mathieu, J. Allegre, A. Chatt, P. Lefebvre, and J.P. Faurie. Band offsets and lattice-mismatch effects in strained-layer CdTe/ZnTe superlattices. *Physical Review B*, 38(11):7740, 1988.

[26] F. Capasso and A.Y. Cho. Bandgap engineering of semiconductor heterostructures by molecular beam epitaxy: physics and applications. *Surface Science*, 299300(0):878 – 891, 1994.

[27] M.S. Jang, S.H. Oh, J.C. Choi, H.L. Park, D.C. Choo, M. Jung, D.U. Lee, and T.W. Kim. Dependence of the activation energies on the well width in CdTe/ZnTe strained single quantum wells. *Solid State Communications*, 121(910):571 – 574, 2002.

[28] Y.H. Kim, I.J. Kim, S.D. Lee, K.N. Oh, S.K. Hong, S.U. Kim, and M.J. Park. A study of photoluminescence of interface layer of ZnTe/CdTe heterostructures. *Journal of Crystal Growth*, 214/215:225–228, 2000.

[29] D.A.B. Miller. *Quantum Mechanics for Scientists and Engineers*. Cambridge University Press, New York, 2008.

[30] C. Weisbuch and B. Vinter. *Quantum Semiconductor Structures - Fundamentals and Applications*. Academic Press, San Diego, 1991.

[31] S. Jovanovic. Pulsed laser heteroepitaxy of high quality CdTe thin films on sapphire substrates. Master's thesis, McMaster University, Hamilton, 2013.

[32] E.R. Dobrovinskaya, L.A. Lytvynov, and V. Pishchik. *Sapphire: Material, Manufacturing, Applications*. Springer Science + Business Media, New York, 2009.

[33] S. Neretina, Q. Zhang, R.A. Hughes, J.F. Britten, N.V. Sochinskii, J.S. Preston, and P. Mascher. The role of lattice mismatch in the deposition of CdTe thin films. *Journal of Electronic Materials*, 35(6):1224–1230, 2006.

[34] S. Neretina, R.A. Hughes, J.F. Britten, N.V. Sochinskii, J.S. Preston, and P. Mascher. The role of substrate surface termination in the deposition of (111) CdTe on (0001) sapphire. *Applied Physics A*, 96(2):429–433, 2009.

[35] M. Konagai, M. Sugimoto, and K. Takahashi. High efficiency GaAs thin film solar cells by peeled film technology. *Journal of Crystal Growth*, 45(0):277 – 280, 1978.

[36] C.W. Cheng, K.T Shiu, N. Li, S.J. Han, L. Shi, and D.K. Sadana. Epitaxial lift-off process for gallium arsenide substrates and flexible electronics. *Nature Communications*, 4:1–7, 2013.

[37] A. Rajan, I.A. Davidson, R.T. Moug, and K.A. Prior. Epitaxial lift-off of IIVI semiconductors from IIIV substrates using a MgS release layer. *Journal of Applied Physics*, 114(24):243510, 2013.

[38] S. Park, Y. Xiong, R. Kim, P. Elvikis, M. Meitl, D. Kim, J. Wu, J. Yoon, C. Yu, Z. Liu, et al. Printed assemblies of inorganic light-emitting diodes for deformable and semitransparent displays. *Science*, 325(5943):977–981, 2009.

[39] P.R. Willmott and J.R. Huber. Pulsed laser vaporization and deposition. *Reviews of Modern Physics*, 72(1):315–328, 2000.

[40] P. Hu, B. Li, L. Feng, J. Wu, H. Jiang, H. Yang, and X. Xiao. Effects of the substrate temperature on the properties of CdTe thin films deposited by pulsed laser deposition. *Surface and Coatings Technology*, 213(0):84 – 89, 2012.

[41] J.G. Lunney. Pulsed laser deposition of metal and metal multilayer films. *Applied Surface Science*, 86(1):79–85, 1995.

[42] D.H.A. Blank, M. Dekkers, and G. Rijnders. Pulsed laser deposition in twente: from research tool towards industrial deposition. *Journal of Physics D: Applied Physics*, 47(3):34006, 2014.

[43] R.D. Vispute, S. Choopun, R. Enck, A. Patel, V. Talyansky, R.P. Sharma, T. Venkatesan, W.L. Sarney, L. Salamancariba, S.N. Andronescu, A.A. Iliadis, and K.A. Jones. Pulsed laser deposition and processing of wide

band gap semiconductors and related materials. *Journal of Electronic Materials*, 28(3):275–286, 1999.

[44] B.B. He. *Two-dimensional X-ray diffraction*. John Wiley & Sons, Hoboken, 2009.

[45] J.I. Pankove. *Optical Processes in Semiconductors*. Dover, New York, 1975.

[46] N. Ghobadi. Band gap determination using absorption spectrum fitting procedure. *International Nano Letters*, 3(1):1–4, 2013.

[47] E.R. Shaaban, I. Kansal, S.H. Mohamed, and J. M.F. Ferreira. Microstructural parameters and optical constants of ZnTe thin films with various thicknesses. *Physica B: Condensed Matter*, 404(20):3571 – 3576, 2009.

[48] J. Tauc. Optical properties and electronic structure of amorphous Ge and Si. *Materials Research Bulletin*, 3(1):37–46, 1968.

[49] User guidlines and standard operating procedure for the cary 50 uv-vis spectrophotometer.

[50] W. Zhou and Z.L. Wang. *Scanning Electron Microscopy for Nanotechnology: Techniques and Applications*. Springer Science + Business Media, New York, 2006.

[51] D.J. O'Connor, B.A Sexton, and R.St.C (Eds) Smart. *Surface Analysis Methods in Materials Science*. Springer-Verlag, Berlin, 2003.

[52] R. Schneider. Electron-energy loss spectroscopy (EELS). In H. Bubert and H. Jenett, editors, *Surface and Thin Film Analysis - A Compendium of Principles, Instrumentaiton, and Applications*, pages 50–70. Wiley - VCH, 2002.

[53] L. Reimer. *Transmission Electron Microscopy: Physics of Image Formation*. Springer Science + Business Media, New York, fifth edition, 2008.

[54] P. Eaton and P. West. *Atomic Force Microscopy.* Oxford University Press, New York, 2010.

[55] S.J. Pennycook, A.R. Lupini, M. Varela, A.Y. Borisevich, Y. Peng, M.P. Oxley, K. van Benthem, and M.F. Chisholm. Scanning transmission electron microscopy for nanostructure characterization. In W. Zhou and Z.L. Wang, editors, *Scanning Microscopy for Nanotechnology, Techniques and Applications*, pages 152–191. Springer Science + Business Media, 2006.

[56] R.F. Egerton. *Electron-Energy Loss Spectroscopy in the Electron Microscope.* Springer, Boston, 2011.

[57] H. Bubert and J.C. Riviere. Auger electron spectroscopy (AES). In H. Bubert and H. Jenett, editors, *Surface and Thin Film Analysis - A Compendium of Principles, Instrumentaiton, and Applications*, pages 32–50. Wiley - VCH, 2002.

[58] G. Friedbacher. Scanning probe microscopy. In H. Bubert and H. Jenett, editors, *Surface and Thin Film Analysis - A Compendium of Principles, Instrumentaiton, and Applications*, pages 276–284. Wiley - VCH, 2002.

[59] R. Howland and L. Benatar. *A practical guide to Scanning Probe Microscopy.* ThermoMicroscopes, 1998.

[60] R. Triboulet and P. Siffert. *CdTe and Related Compounds; Physics, Defects, Hetero- and Nano-structures, Crystal Growth, Surfaces and Applications*, volume 1. Elsevier, Oxford, 2010.

[61] B. Kotlyarchuk and V. Savchuk. Investigation of ZnTe thin films grown by pulsed laser deposition method. *Physica Status Solidi (B)*, 244(5):1714–1719, 2007.

[62] S. Adachi. *Optical Constants of Crystalline and Amorphous Semiconductors.* Kluwer Academic Publishers, Massachusetts, 1999.

[63] X.J. Wang, Y. Chang, C.R. Becker, C.H. Grein, S. Sivananthan, and R. Kodema. Microstructure of heteroepitaxial ZnTe grown by molecular beam epitaxy on Si(211) substrates. *Journal of Electronic Materials*, 40(8):1860–1866, 2011.

[64] A. Hamoudi, E. Ligeon, K. Saminadayar, J. Cibert, L.S. Dang, and S. Tatarenko. Annealing effect on the shape of CdTe/ZnTe quantum wells. *Applied Physics Letters*, 60(22):2797–2799, 1992.